Chem Soc Rev

Functionalised tetrathiafulvalene- (TTF-) macrocycles: Recent trends in applied supramolecular chemistry

Journal:	*Chemical Society Reviews*
Manuscript ID	CS-SYN-01-2018-000035.R2
Article Type:	Review Article
Date Submitted by the Author:	27-Jun-2018
Complete List of Authors:	Jana, Atanu; Shanghai University Bähring, Steffen; Department of Chemistry, SDU: Odense University Ishida , Masatoshi ; KYUSHU UNIVERSITY Goeb, Sebastien; Universite d' Angers, CNRS UMR 6200 - MOLTECH ANJOU Canevet, David; Université d'Angers, MOLTECH-ANJOU, UMR CNRS 6200 Salle, Marc; Université d'Angers, MOLTECH-Anjou, UMR CNRS 6200 Jeppesen, Jan Oskar; Department of Chemistry, SDU: Odense University Sessler, Jonathan; Univ Texas Austin, Chemistry; Shanghai University,

Journal Name

ARTICLE

Functionalised tetrathiafulvalene- (TTF-) macrocycles: Recent trends in applied supramolecular chemistry

Received 00th January 20xx,
Accepted 00th January 20xx

DOI: 10.1039/x0xx00000x

www.rsc.org/

Atanu Jana,[a] Steffen Bähring,[b] Masatoshi Ishida,[c] Sébastien Goeb,[d] David Canevet,[d] Marc Sallé,*[d] Jan O. Jeppesen*[b] and Jonathan L. Sessler*[ae]

Tetrathiafulvalene (TTF) has been extensively explored as a π-electron donor in supramolecular systems. Over the last two decades substantial advances have been made in terms of constructing elaborate architectures based on TTF and in exploiting the resulting systems in the context of supramolecular host–guest recognition. The inherent electron-donating character of TTF derivatives has led to their use in the construction of highly efficient optoelectronic materials, optical sensors, and electron-transfer ensembles. TTFs are also promising candidates for the development of the so-called "functional materials" that might see use in a range of modern technological applications. Novel synthetic strategies, coupled with the versatility inherent with the TTF moiety, are now allowing the architecture of TTF-based systems to be tuned precisely and modified for use in specific purposes. In this critical review, we provide a "state-of-the-art" overview of research involving TTF-based macrocyclic systems with a focus on their use in supramolecular host–guest recognition, as components in non-covalent electron transfer systems, and in the construction of "molecular machines".

1. Introduction

Since the revolutionary discovery of the first conducting "organic metals" based on tetrathiafulvalene (TTF), including [$TTF^{\bullet+}/Cl^{-}$][1,2] and [TTF/TCNQ],[3] in the early 1970's, a large number of TTF derivatives have been reported in the literature. In fact, to date, over seven thousand papers have been published on the synthesis, functionalisation, or use of TTF derivatives as inferred from a Scifinder Scholar search using the key word "*tetrathiafulvalene*". TTF subunits are of particular interest as potential electron donors in charge-transfer (CT) complexes intended for use in a variety of applications, including electrochemical switches, electron transfer ensembles and sensors. Several reviews outlining these applications have been published in recent years.[4–20]

A separate broad theme within the context of TTF chemistry involves the design and synthesis of receptor systems that incorporate this quintessential redox active moiety. Among this generalised class of hosts, TTF-annulated macrocyclic compounds occupy a central position. This importance reflects in part the fact that they can act as "functional materials" that display redox active features and which respond to various environmental inputs. This has permitted the construction of macrocyclic systems that recognise anions, explosives and certain other guest molecules. Switchable behaviour, particularly an ability to encapsulate, bind, and reversibly release guest molecules, as well as support colourimetric and electrochemical sensing, are often hallmarks of these systems. However, reviews focused on this aspect of TTF chemistry are all but non-existent. Therefore, the goal of this Critical Review is to highlight some of the most salient applications of TTF-based macrocyclic systems including cage systems and their functional features. Also included is a brief discussion of TTF-catenane based "molecular machines".

2. Scope of this review

There are several reviews highlighting the TTF-oligomers bearing different functionalities,[7–12,21–24] as well as one focused on TTF-cyclophanes and cage-motifs.[25] Reviews summarising the chemistry of TTF-based donor–acceptor (D–A) ensembles and their potential application as molecular materials and devices have also appeared.[26–28] However, the reviews in question are not recent (*i.e.*, published ≥10 years ago) and they do not provide coverage of relatively new and often quite complex systems. A review article was recently published by some of the present authors.[20] However, this latter review was focused exclusively on TTF-based polypyrrolic systems and did not highlight TTF-based supramolecular receptors. The present review is designed to address this latter coverage

[a]*Institute for Supramolecular Chemistry and Catalysis, Shanghai University, Shanghai, 200444, China.*
[b]*Department of Physics, Chemistry and Pharmacy, University of Southern Denmark, Campusvej 55, 5230, Odense M, Denmark. E-mail: joj@sdu.dk Telephone: +45-65502587.*
[c]*Department of Chemistry and Biochemistry, Graduate School of Engineering and Center for Molecular Systems, Kyushu University, Fukuoka 819-0395, Japan*
[d]*Université d'Angers, CNRS UMR 6200, Laboratoire MOLTECH-Anjou, 2 bd Lavoisier, 49045 Angers Cedex, France. E-mail : marc.salle@univ-angers.fr Telephone: +33-241735439.*
[e]*Department of Chemistry, University of Texas at Austin, Austin, Texas 78712-1224, USA. E-mail: sessler@cm.utexas.edu Telephone: +1-512-471-5009.*
† Footnotes relating to the title and/or authors should appear here.
Electronic Supplementary Information (ESI) available: [details of any supplementary information available should be included here]. See DOI: 10.1039/x0xx00000x

lacuna and to highlight the potential of TTF-based receptors to act as "functional materials".

TTF-fused macrocyclic systems have attracted considerable attention as potential receptors for electron poor guests, such as nitroaromatic explosives. Other TTF-derived systems have unique bowl-like shapes that allow them to encapsulate and separate spherical guests, such as C_{60}. Some of the TTF-based systems reported in recent years have been found to act as electron reservoirs that function as readily controllable electron donors. The goal of this present review is to provide a general overview that will summarise the state-of-the-art in TTF-based macrocycle chemistry while providing a foundation for the design of the next generation of "functional materials" containing electroactive TTF-moieties. In this context, our goal is to summarise the chemistry and applications of various TTF-based macrocyclic compounds, including TTF-calix[4]pyrroles, so-called exTTF-porphyrins/macrocycles, TTF-carcerands, TTF-hemicarcerands, TTF-cryptands, as well as TTF-based metalla-macrocyclic systems. We also review the various design strategies that have led to the synthesis of "functional materials" and electroactive "molecular machines". Throughout the treatment, a key focus will be on potential applications.

In the first part of this review, we describe various TTF- (and exTTF-) annulated macrocyclic systems and their applications in host–guest chemistry. The second part is dedicated to organic TTF- (and exTTF-) based cage systems (including metalla-cages) and their ability to bind electron poor guests by means of supramolecular D–A type interactions. In this section, the electrochemical and photophysical effects associated with guest binding are discussed. Finally, we outline the design strategies used to prepare electroactive "molecular machines" based on macrocyclic systems containing TTF subunits. In this context, interlocked molecular architectures, *e.g.*, catenanes will receive particular emphasis.

3. TTF-based macrocyclic systems

As described in the introduction, tremendous efforts have been made to attach electroactive TTF moieties to classic macrocyclic motifs to produce hybrid molecular systems. For example, TTF(s) have been grafted onto the periphery of crown ethers, cryptands and calixpyrroles to make increasingly complex structures. This has provided electroactive macrocyclic systems that retain the core molecular recognition features of the parent macrocycles. On the other hand, the TTF moieties incorporated in this way function as transducers that respond to external inputs (stimuli), thus producing a change in the overall electronic features of the system. This change can be typically detected by electrochemical or spectroscopic means. The result can be elaborated receptor systems with considerable sensing capability.

3.1. TTF-calixpyrroles as anion sensors. Annulation of TTF derivatives onto a pyrrole subunit through the β,β' positions provides useful new building blocks that can impart both rigidity and electron-donating character to a range of polypyrrolic macrocycles (*e.g.*, porphyrins, phthalocyanines, subphthalocyanines, calixpyrroles, *etc.*). When incorporated into a calix[*n*]pyrrole (*n* = 4, 5 and 6) framework, higher binding affinities toward anions are observed as the result of increased NH–anion hydrogen-bonding interactions.[29] The peripheral TTF subunits are inherently electron-rich. They can thus provide ancillary sites for guest recognition. The underlying shape of the system can play a role. For instance, clip-like systems that adopt tweezers-type geometries are potential hosts for many planar electron deficient guests. Often the resulting host–guest supramolecular complexation and sensing behaviour is reflected in noticeable colour changes under ambient conditions.

The chemistry of TTF-calix[4]pyrrole-based anion sensors was originally developed by Becher, Jeppesen and Sessler and has been thoroughly reviewed recently.[20] Nevertheless, a brief discussion is appropriate here. The chemical structures of few representative TTF-based macrocyclic systems are given in Chart 1. Of these, compounds **1**–**6** are potential electrochemical sensors for ionic substrates.[30,31] Receptor **4** is particularly noteworthy; it displays several exciting chemical and photophysical features that were ascribed in large measure to its ability to adopt two different limiting conformations *viz*. the (a) 1,3-alternate and the (b) cone-like conformers in the absence and presence of anions, respectively. In the absence of anions, the 1,3 alternate form is energetically favourable as is the case for most other calix[4]pyrroles. In contrast, in the presence of coordinating anions, such as Cl^-, these systems adopt the corresponding cone conformation, a change that is ascribed to strong hydrogen-bonding interactions between the pyrrolic NH protons and the bound anionic guest (Fig. 1).

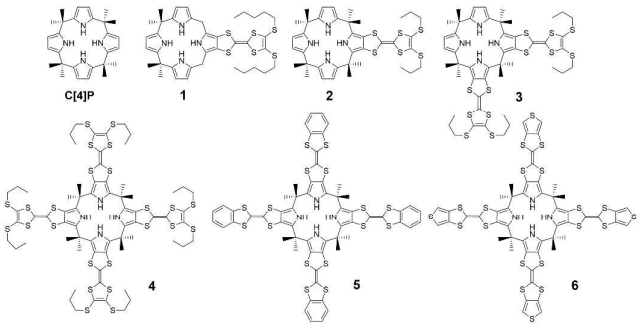

Chart 1 Chemical structures of various TTF-based calix[4]pyrrole receptors (**1**-**6**) and the corresponding reference compound octamethyl-calix[4]pyrrole, C[4]P.

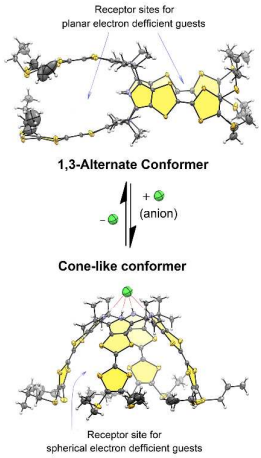

Fig. 1 Two distinct conformers of *tetrakis*-TTF-calix[4]pyrrole, **4**. The conversion between the 1,3-alternate and cone-like conformers is driven by anion recognition. (This figure is redrawn based on one that originally appeared in reference 32.)

3.2. TTF-based calix[4]pyrroles as sensors for neutral electron-deficient aromatic guests. The TTF-based calix[4]pyrrole system, **4**, also acts as an effective receptor for electron deficient planar nitroaromatic compounds, including 1,3,5-trinitrobenzene (TNB), tetrafluoro-*p*-benzoquinone, tetrachloro-*p*-benzoquinone and *p*-benzoquinone, in dichloromethane solution.[32] The underlying neutral substrate recognition requires the 1,3-conformer. It can thus be blocked by the addition of chloride anion, which serves to induce a conformational change to the cone-like form as shown in Fig. 1. The 1,3-alternate conformation of receptor **4** binds a number of electron-deficient guests in a 1:2 host–guest stoichiometry. The resulting complexes adopt sandwich-like structures with stabilisation provided *via* D–A–D-based CT interactions (Fig. 2). A characteristic intermolecular CT band at λ_{max} = 677 nm in the Vis–NIR absorption spectrum, was observed when **4** was treated with TNB and related explosive materials in CH_2Cl_2 at 298 K. Addition of Cl^- anion was found to trigger conversion to the cone conformation and release of the guest.

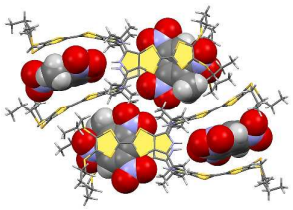

Fig. 2 Single crystal X-ray structure of the supramolecular complex **4**•TNB_2. (This figure was redrawn using data that were originally published in reference 32.)

Positive homotropic allosteric binding properties of TTF-calix[4]pyrrole derivatives with electron-deficient guests. Compound **4** was also found to bind well 1,4,5,8-naphthalenetetracarboxylic dianhydride (NDA). As true for the poly-nitroaromatic explosives noted above, a 1:2 (receptor:guest) stoichiometry was observed in organic solvents in the absence of a coordinating anion, such as Cl^-.[33] Absorption data from a spectroscopic titration carried out in CH_2Cl_2 was fitted to a two-site Adair equation; this provided two microscopic binding constants, K_1 = 2.9 × 10^4 M^{-1} and K_2 = 1.0 × 10^6 M^{-1}, respectively, (K_a = 2.9 × 10^{10} M^{-2}) in the case of NDA. A reverse fluorescence-based titration provided support for the high affinities, which proved to be the highest reported at the time for a TTF-calixpyrole macrocyclic host and a guest. Another two TTF-based calix[4]pyrroles, *viz*. **5** and **6**, were also described[34] and their ability to bind nitroaromatic explosives, including TNB, picric acid (TNP) and 2,4,6-trinitrotoluene (TNT), was explored. A careful analysis of the colourimetric changes observed when TNB, TNP and TNT, were allowed to react with **5** and **6** in $CHCl_3$ revealed a positive homotropic allosteric effect (*i.e.*, K_1<K_2).[34] Fig. 3 illustrates the proposed origin of this positive homotropic allosteric effect observed in the case of receptors **4** and **5** with NDA and TNP, respectively. Briefly, binding of the first guest leads the inherently flexible host systems to adopt a 1,3-alternate conformation. This results in formation of a preorganised structure that is able to encapsulate more effectively the second guest molecule. A summary of the binding parameters derived from quantitative analyses of visible spectroscopic titration data is provided in Table 1.

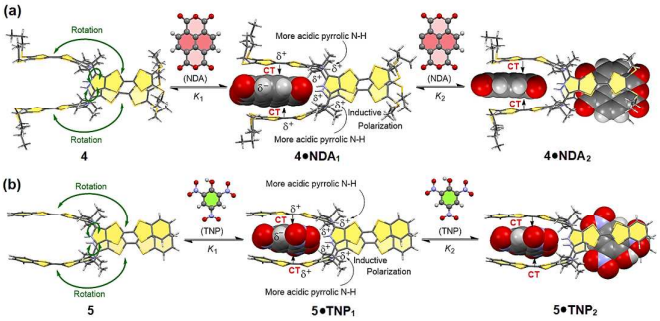

Fig. 3 Proposed origin of the positive homotropic allosteric effect observed in the case of receptors **4** and **5** when allowed to react with the electron deficient guests NDA and TNP. (This figure was redrawn using data that were originally published in references 33 and 34.)

Table 1 Association constants[a,b] and cooperativity parameters observed for macrocycles **4**, **5**, and **6** when used as receptors for TNB, TNP, TNT and NDA.

Comp	K_a(M^{-2})	N	K_1(M^{-1})	K_2(M^{-1})	K_2/K_1
4•TNB_2	4.3×10^3	1.27	3.9×10^2	1.4×10^3	3.6
4•TNP_2	3.8×10^3	1.30	2.8×10^2	1.2×10^3	4.1
4•TNT_2	3.3×10^2	1.23	5.9×10^1	2.0×10^2	3.3
4•NDA_2[c]	2.9×10^{10}	–	2.9×10^4	1.0×10^6	34.5
5•TNB_2	1.5×10^5	1.34	2.8×10^3	1.7×10^4	6.2
5•TNP_2	9.1×10^4	1.34	1.7×10^3	1.1×10^4	6.5
5•TNT_2	1.2×10^4	1.31	5.7×10^2	2.6×10^3	4.5
6•TNB_2	3.4×10^6	1.70	1.3×10^3	3.1×10^4	24
6•TNP_2	3.7×10^6	1.86	6.4×10^2	2.0×10^4	31
6•TNT_2	2.3×10^4	1.45	3.2×10^2	2.8×10^3	10

[a]Based on absorption spectroscopic titrations of the respective hosts (0.20 mM) in $CHCl_3$ at 298 K. [b]The estimated errors for the reported binding constants are ≤12%. [c]These data based on the absorption spectroscopic titration of 5.6 μM host (**4**) with NDA in CH_2Cl_2 at 298 K.

Several reports have appeared[35,36] of molecular devices that exploit the positive homotropic allosteric binding features that receptor **4** displays towards electron poor aromatic guests. The

systems in question proved capable of effecting the stand-off detection of nitroaromatic explosive vapours. In fact, a detection limit of less than 10 ppb of TNB vapour was achieved using a polymer microcantilever system.[35]

Recently, Flood and co-workers reported[37] a more efficient detection technique for nitroaromatic explosives that is based on the use of a "turn-ON" resonance Raman spectroscopic signal. These researchers exploited the CT chromophore that arises from the host–guest supramolecular complexation of **4** with *e.g.*, TNB by exciting the complex with a laser at λ = 785 nm. According to the authors, this approach allows for the selective and efficient detection of nitroaromatic explosives with a fingerprint unique to the specific substrates. Solution and solid state measurements of the host–guest chromophore complexes revealed that the signal strength of the nitro groups being monitored is increased by a factor of 10–20 relative to the isolated nitroaromatic analytes as the result of supramolecular complexation. The significant enhancement of the intensity (Fig. 4) of the nitro group vibrations arising from complexation is ascribed to a constructive resonance between the applied 785 nm laser light and the CT chromophore of the complex (*i.e.*, **4**•TNB_2). This report represents an important step forward in that it shows that a properly constructed TTF-based receptor combined surface-enhanced spectroscopic techniques may provide a means for detecting nitroaromatic explosives with increased sensitivity and selectivity. As might be expected, addition of a Cl^- anion salt regenerates the cone-like conformation. This expels the TNB guest and constitutes a stimulus-induced change that in principle sets up the system for further use or reuse.

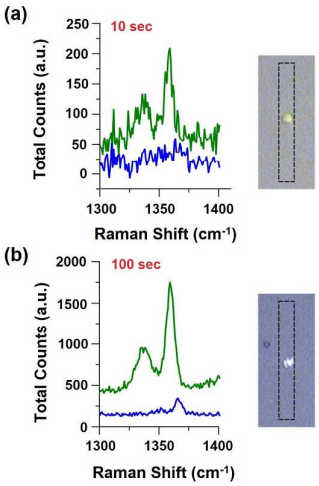

Fig. 4 Solid-state resonance Raman spectra (λ_{exc} = 785 nm) recorded at room temperature of microcrystalline samples of **4**•TNB_2 (green) and TNB (blue). Also shown are the corresponding microscopic images of 1 mm^3 samples of **4**•TNB_2 and TNB showing the dimensions (dotted lines) of the laser spot (2.5 mm 28 mm) observed upon exposure to a 0.3 mW laser light source for (a) 10 s and (b) 100 s, respectively. (Reproduced from reference 37 with permission from The Royal Society of Chemistry, copyright 2017).

3.3. TTF-based calix[4]pyrroles for sensing spherical guests. Sessler and Jeppesen *et al.* also demonstrated a self-assembled multicomponent molecular host system[38,39] based on **4** that was found to interact with the electron-deficient acceptor C_{60} in the presence of chloride anion. It was demonstrated that no significant absorption was observed for receptor **4** or the C_{60} guest molecule in CH_2Cl_2 beyond $\lambda_{max} \geq 550$ nm. However, when C_{60} was added to receptor **4** in the presence of a Cl^- anion source, the colour of the solution was found to turn green immediately on the laboratory time scale; this change in colour was ascribed to conversion of the initial 1,3-alternate structure to the corresponding bowl shaped cone conformer and formation of an ordered multicomponent supramolecular ensemble.

The absorption spectrum of the complex, which was subsequently assigned as C_{60}⊂**4**•Cl^-, is characterised by a strong CT band with a λ_{max} = 725 nm (Fig. 5a, curve iv). In contrast, the addition of two equiv. of receptor **4** in its anion-free 1,3-alternate conformation to a solution of C_{60} in CH_2Cl_2 produces a brown solution. This solution is characterised by the presence of a weak, broad absorption band centred at λ_{max} = 748 nm (ε = 500 $M^{-1}cm^{-1}$) in the visible spectral region (Fig. 5a, curve iii). Such features are consistent with only minimal intermolecular interactions between C_{60} and **4**. However, the addition of five equiv. of tetrabutylammonium chloride (TBACl) as a Cl^- source to this mixture of **4** and C_{60} resulted in an instantaneous colour change from brown to green and the appearance of a strong CT absorption band (Fig. 5a, curve v) centred at λ_{max} = 725 nm; ε = 1900 $M^{-1}cm^{-1}$). Such a finding provides support for the proposal that C_{60} is only encapsulated after **4** undergoes a change from the 1,3-alternate conformation to the corresponding chloride-bound cone conformation (*i.e.*, **4**•Cl^-). Single crystal X-ray diffraction analyses of crystals grown in the presence of tetraoctylammonium chloride (TOACl) provide support for the proposed 1:1 binding stoichiometry between receptor **4** and the C_{60} guest yielding a complex with the empirical formula (TOA)[C_{60}⊂(**4**•Cl)]. A view of this supramolecular complex is provided in Figure 5b.

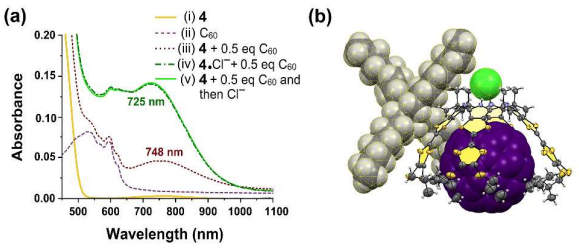

Fig. 5 (a) Vis–NIR spectra of (i) **4**, (ii) C_{60}, (iii) a mixture of **4** and 0.5 equiv. of C_{60}, (iv) the putative complex with C_{60} produced after the addition of 0.5 equiv. of C_{60} to the **4**•Cl^-, and (v) a mixture of **4** and 0.5 equiv. of C_{60} in the presence of excess TBACl. All spectroscopic measurements were carried out in CH_2Cl_2 at 298 K. This figure is reproduced with permission from reference 38. Copyright 2006 WILEY-VCH Verlag GmbH; (b) Single crystal X-ray diffraction structure of (TOA)[C_{60}⊂(**4**•Cl)], TOA^+ = tetraoctylammonium cation. This figure is redrawn using data originally published in reference 39.

Jeppesen, Guldi and Sessler *et al.* reported several environmentally responsive, multicomponent supramolecular

switching devices made up from receptor **4** and judiciously chosen neutral guest molecules.[40,41] The guests used for these studies included planar or quasi-planar nitroaromatic guests, such as TNB (**A**), methyl-2,5,7-trinitrofluorenone-4-carboxylate (**B**), methyl-2,5,7-trinitrodicyanomethylenefluorene-4-carboxylate (**C**) as well as the spherical substrates fullerene C_{60} (**D**) and its derivative *N*-methylfulleropyrrolidine (**E**) (*cf*. Scheme 1).

To investigate the effect of the individual chemical inputs, **C** and **E** were added to the receptor system **4** in the absence as well as in the presence of anions. It was observed that, after addition of 2.0 molar equiv. of **A** (0.8 mM) and 0.5 equiv. of **E** (0.2 mM) to a 0.4 mM CH_2Cl_2 solution of receptor **4**, the colour changed from yellow to brown almost instantaneously on the laboratory time scale. This visual colour change was ascribed to the formation of a complex, $\mathbf{C}_2\subset\mathbf{4}$, wherein receptor **4** resides in its 1,3-alternate conformation. The absorption spectrum of this presumed complex displayed CT bands centred at λ_{max} = 525, 720 and 1220 nm (ε = 3700, 2000 and 2800 M^{-1} cm^{-1}), respectively.[40] Addition of 2 equiv. of a chloride anion source to this solution results in a conformational change of the receptor **4** from the 1,3-alternate to the corresponding cone conformation $\mathbf{4}\bullet Cl^-$. As a consequence, the 2:1 complex $\mathbf{C}_2\subset\mathbf{4}$ breaks up and is replaced by a 1:1 receptor–fullerene stoichiometry with an empirical formula of $\mathbf{E}\subset\mathbf{4}\bullet Cl^-$ (Scheme 1).

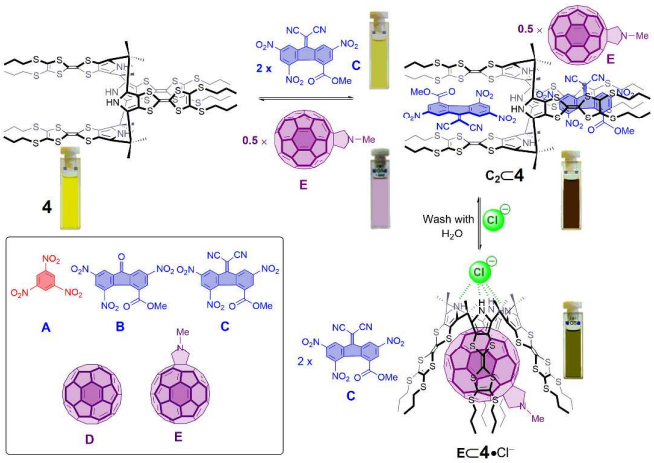

Scheme 1 Binding modes seen for receptor **4** when exposed to different substrates (**A**–**E**) in the presence and absence of a chloride anion source.

3.4. Ion-mediated reversible electron transfer (ET) processes involving supramolecular ensembles formed between TTF-based calix[4]pyrroles and electron-deficient guests. Anion-mediated reversible electron transfer (ET) in a synthetic TTF-calix[4]pyrrole based host–guest assembly was reported by Sessler and co-workers.[42] As with other calix[4]pyrrole ensembles, in this case anion binding to receptor **4** stabilises a cone conformer that can act as a receptor for large cationic guests, *i.e.*, the electron-deficient benzimidazolium quinone (BIQ^{2+}). The resulting complex undergoes intra-ensemble thermal electron transfer to produce a long-lived charge separated (CS) state. Based on an X-ray structural analysis, this supramolecular capsule is best described as a tightly coupled biradical species, $[\mathbf{4}]_2^{\bullet+}\bullet BIQ^{\bullet+}\bullet 2Cl^-$, wherein two cone-like anion-bound conformers of **4** (one of which is oxidised by one electron) serve to encapsulate the one-electron reduced form of the guest, $BIQ^{\bullet+}$ (Fig. 6).

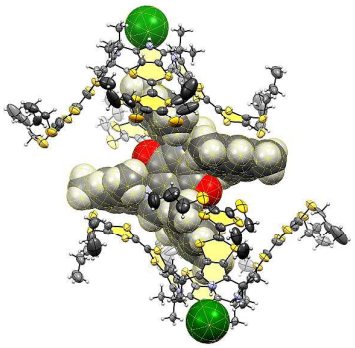

Fig. 6 X-ray crystal structure of the Cl^- induced supramolecular radical ion pair capsule complex obtained by mixing **4** with BIQ^{2+} in the presence of an appropriate chloride anion source. The complex has a net stoichiometry of $[\mathbf{4}]_2^{\bullet+}\bullet[BIQ]^{\bullet+}\bullet 2Cl^-$. (This figure was redrawn using data that were originally published in references 42.)

Another example of anion induced reversible ground state electron transfer involving receptor **4** was also demonstrated[43] by Fukuzumi, Kim and Sessler *et al*. using $Li^+@C_{60}$ as the electron acceptor. In this three-component supramolecular system, the ET is switched "ON" upon addition of a Cl^- anion source to the host **4** with $Li^+@C_{60}$. However, addition of the tetraethylammonium cation (TEA^+ as, *e.g.*, TEACl) introduces a relatively small cation that acts as a competitive inhibitor for the $Li^+@C_{60}$ guest. This latter species is thus excluded from the cavity, resulting in effective switching "OFF" of the ET event.

Photoinduced electron transfer (PET) from an electron-rich TTF-calix[4]pyrrole, **5**, to a porphyrin carboxylate, PA, within a supramolecular triad (Fig. 7a) was also reported.[44] Here, TEA^+ was chosen as the counter-cation to the carboxylate moiety. As above, this cation is bound inside the cavity of **5** when it is in its cone conformation (as induced by carboxylate anion complexation to the calix[4]pyrrole NH protons). This dual binding, involving the complexation of both TEA^+ and the carboxylate moiety to receptor **5**, was expected to enhance the interaction between the PA and **5** leading to stronger supramolecular complexation. Laser photoexcitation of this supramolecular complex results in formation of a triplet CS state composed of a $TTF^{\bullet+}$ radical cation and a radical anion $PA^{\bullet-}$.

Another example of a three component supramolecular ensemble undergoing photoinduced electron transfer (PET) was also reported (Fig. 7b).[45] In this case, $Li^+@C_{60}$ was used in conjunction with **5** and a different porphyrin carboxylate anion, PA_2. Photoexcitation of the three component mixture results in PET from the triplet excited state of PA_2 to $\mathbf{5}^{\bullet+}$. A characteristic signal at 1035 nm in the Vis–NIR absorption spectra is consistent with the formation of a CS species, $\mathbf{5}^{\bullet+}/Li^+@C_{60}^{\bullet-}$, where the PA_2 is in its neutral form. These findings were taken as support for the

conclusion that the three components undergo self-assembly to produce a multi-component redox active ensemble.

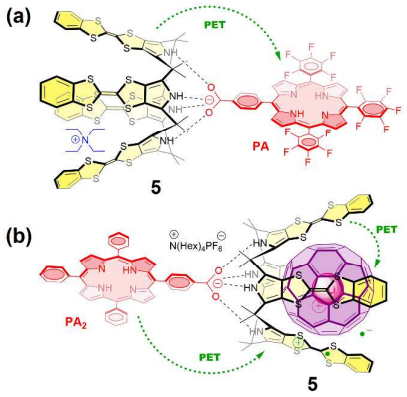

Fig. 7 Schematic representation of the photoinduced electron transfer (PET) proposed to occur within supramolecular ensembles formed from the electron-rich TTF-calix[4]pyrrole **5** and electron-deficient porphyrin carboxylate salts. (a) PET from electron-rich **5** to PA. (b) Dual PET from both **5** and PA_2 to electron-deficient $Li^+@C_{60}$.

3.5. Recognition of explosive materials and other electron deficient guests within "Pacman" type receptors. The TTF-calix[2]thiophene[2]pyrrole (**7**) is another macrocyclic host system reported by Sessler *et al.*[46] This receptor was found to bind certain electron-deficient planar guest molecules in a Pacman-like fashion (Chart 2). The system acts as a chemosensor and, in analogy to what was seen for **4**, gives rise to a readily visible colour change in the presence of nitroaromatic analytes, such as TNB and picric acid. A solid state structural analysis of one such host–guest supramolecular complex (Figs. 8a,b) established a "cleft-like" arrangement wherein the two TTF units lie parallel to one another and are separated by approximately 3.44–3.56 Å.

Jeppesen *et al.* reported[47] a TTF-calix[2]pyrrole[2]thiophene hybrid system, **8**, wherein two thiophene moieties are incorporated into the central macrocyclic skeleton. This system was found to act as a molecular receptor for another planar guest, namely 7,7,8,8-tetracyano-*p*-quinodimethane (TCNQ). Again, a Pacman-like binding arrangement was seen in the solid state (Figs. 8c,d).

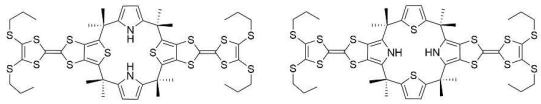

Chart 2 Chemical structures of the *bis*-TTF-calix[2]thiophene[2]pyrrole (**7**) and *bis*-TTF-calix[2]pyrrole[2]thiophene (**8**) receptors.

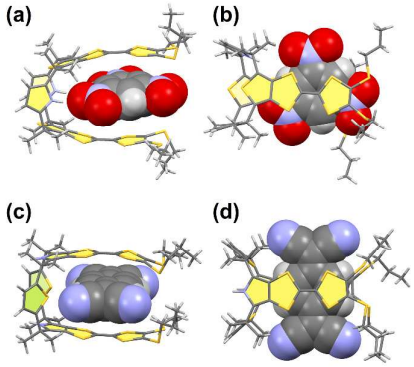

Fig. 8 Solid state structures of the *bis*-TTF-calix[2]thiophene[2]pyrrole, **7**, showing the Pacman-like binding mode observed upon complexation of a TNB guest (a) side view; (b) top view. Solid state structures of the TCNQ complex of the *bis*-TTF-calix[2]pyrrole[2]thiophene, **8**. (c) View along the crystallographic 'a' axis; (d) view along the 'b' axis. (This figure was redrawn using data that were originally published in references 46 and 47.)

4. ExTTF-based macrocyclic systems

So-called exTTF systems are the conceptual analogues of TTF moieties wherein the electron rich dithiolylidene subunits are separated from one another. However, in contrast to the nearly planar geometry generally displayed by the TTF subunit, exTTF molecular motifs are often highly distorted and saddle-shaped.[15,48,49] These unique molecular geometries make exTTF systems attractive as potential receptors for suitable spherical guests, such as C_{60}. Interestingly, a one-step two-electron oxidation process results in the production of $exTTF^{2+}$ and a planarisation of the anthracene core bearing the two orthogonal dithiolium moieties at its 9 and 10 positions. This change is accompanied by an inferred gain in aromaticity. On this basis, it was considered likely that this exTTF could act as a potential donor in analogy to what is seen for other conventional donors, *e.g.*, porphyrins, ferrocene, aniline derivatives and π-conjugated oligomers, whose oxidation leads to loss of aromaticity. In this section, we summarise the chemistry of anthraquinone-based exTTF systems, as well as that of super-π-extended tetrathiafulvalene- (sExTTF-) molecular systems.

4.1. Crown ether fused exTTF macrocyclic systems. Crown ether annulated exTTF compounds are a class of molecular motifs that have been used for recognising and sensing fullerenes, as well as metal cations. Bryce *et al*. reported several crown ether annulated 9,10-bis(1,3-dithiol-2-ylidene)-9,10-dihydroanthraquinone exTTF (exTTFAQ) derivatives, *e.g.*, **9a**,**b** and **10a**,**b** respectively[50,51] (see Chart 3), which could be used to sense the Na^+ and Ag^+ cations with selectivity over the Li^+ and K^+ cations. A solid state crystal structure of **9b** revealed a highly curved crown ether–exTTFAQ π-molecular geometry (Fig. 9). It was also anticipated that compound **10a,b** would possess an arc-shaped conformation with a preorganised and rigid inner cavity; such features were expected to enhance the binding of certain cationic species *via* synergistic crown ether–cation and π–cation interactions (*i.e.*, cooperativity).[51]

Detailed electrochemical studies of both **9b** and **10b** revealed that the two-electron oxidation wave anodically shifts (ΔE_1^{ox}) by up to 115 mV when titrated with silver triflate, and 100 mV when titrated with the corresponding sodium salt in MeCN. These changes were taken as evidence for efficient transduction of the cation recognition process into a readily monitored electrochemical event.

These exTTF-based derivatives display an additional one-electron oxidation wave, which was not affected by adding cations. As proposed by the authors, this particular observation reflects loss of the cations from the crown ether upon generation of the dithiolium form. This observation was further supported by Ohta and Fujimori *et al.*, who reported[52] that addition of alkali metal salts to **11a** and **11b** significantly affects their ^{1}H NMR spectra (CD_3CN) in the neutral state. On the other hand, no appreciable changes in the chemical shifts were observed when alkali metal salts were added to the dicationic state. It was suggested that because these crown ether annulated exTTF derivatives allow for the spectrophotometric and electrochemical sensing of metal cations, they could prove useful in the development of chemosensor devices.

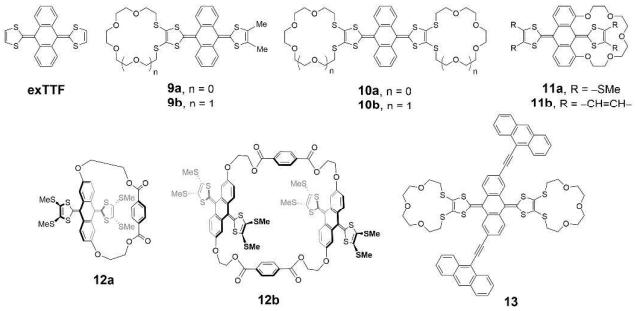

Chart 3 Chemical structures of crown ether annulated exTTFAQ-based receptors.

Another set of electroactive exTTFAQ derivatives, **12a,b**, were also reported by Bryce and co-workers.[53] Single crystal X-ray structural analyses revealed that the exTTFAQ moieties within **12a** and **12b** adopt saddle-shaped conformations as seen in the case of compound **9b** (*cf*. Fig. 9).

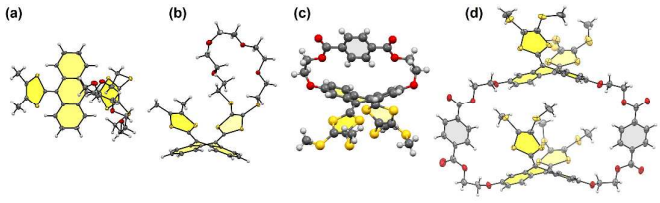

Fig. 9 Single crystal X-ray structures of compounds **9b** (a) front view and (b) side view, **12a** (c), and **12b** (d) respectively, showing what are highly distorted saddle-shaped geometries. Residual solvent molecules are omitted for clarity. This figure was redrawn using data that were originally published in references 50 and 53.

Zhao *et al*. reported[54] a novel fluorescence chemosensor, **13**, (Chart 3) made up of a bis-crown-annulated exTTFAQ receptor and two anthracene fluorophores. A single crystal X-ray diffraction structure revealed a geometry consistent with a highly strained core (Fig. 10). Two crown ether moieties are oriented in the same direction to form a molecular tweezer that was deemed suitable for cation recognition. Fluorescence spectral titrations provided support for this contention in that receptor **13** showed high affinities for large hard metal cations, such as Ba^{2+} (Table 2). The proposed metal binding mode and fluorescence switching mechanism are both shown in Scheme 2.

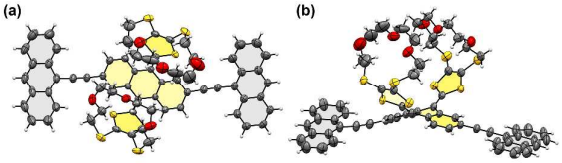

Fig. 10 ORTEP representation (30% probability ellipsoids) of compound **13**. (a) Front and (b) side views. Residual solvent molecules are omitted for clarity. This figure was redrawn using data that were originally published in reference 54.

Table 2 Stability constants[a] derived from fluorescence titration experiments involving treatment **13** with various metal ions (as their triflate salts).

Metal ions	Ionic radius	$\log\beta_{11}(M^{-1})$	$\log\beta_{12}(M^{-2})$
Ba^{2+}	135 pm	4.51 ± 0.42	8.76 ± 0.45
Li^{+}	76 pm	4.25 ± 0.12	6.48 ± 0.26
Ag^{+}	115 pm	5.42 ± 0.17	7.83 ± 0.18

[a]Measurements were performed in THF.

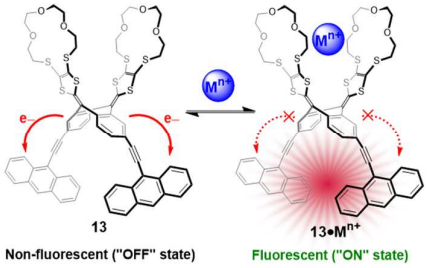

Scheme 2 Proposed interactions between receptor **13** and metal ions. The associated geometrical changes are thought to underlie its ability to act as a fluorescent sensor for the Ba^{2+} cation.

Martín and co-workers reported[55] an exTTF-based macrocyclic system **14** that was found to form pseudorotaxanes through hydrogen bonding interactions with axles **15** and **16**, respectively (*cf*. Chart 4). The same research group also described a terminally attached crown ether–exTTF hybrid system[56] **18** that forms robust supramolecular self-assembled ensembles involving the electron rich exTTF unit and the complementary electron deficient C_{60} derivatives **16** and **17**. For instance, a strong binding was observed upon mixing **18** with **17** (log $K_a \approx 6$ in chlorobenzene (PhCl) or $CHCl_3$ at 298 K). This high affinity was ascribed to both complementary π–π stacking between the concave exTTF unit and the convex fullerene and hydrogen bonding between the crown ether moiety and the ammonium counterpart of **17**. Various spectroscopic and electrochemical measurements provided evidence for CT interactions between the exTTF moiety and the C_{60} guest in the ground state. Transient absorption spectroscopic measurements revealed the photoinduced generation of charge separated (CS) species with a lifetime value of 9.3 ps in PhCl.

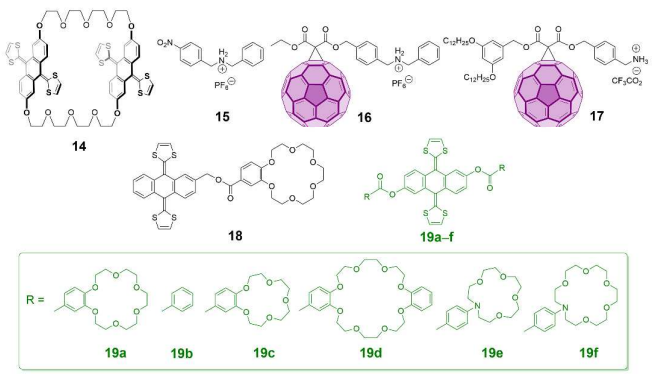

Chart 4 Chemical structures of exTTF-based receptors (**14**, **18** and **19a–f**) and their complementary guests (**15**, **16** and **17**).

Another interesting exTTF-*bis*(crown ether) derivative, **19a**, was reported[57] by Martín and co-workers. This system recognises C_{60} as well as C_{70} efficiently by means of presumed cooperative π–π and n–π interactions. Favourable geometrical (concave–convex) and electronic (donor–acceptor) complementarity was proposed to account for the observed ability to complex fullerenes strongly (association constants reaching 10^7 M^{-1} in benzonitrile (PhCN) at 298 K). Calculations were used to predict the geometries of **19a** when complexed with C_{60} and C_{70}. The results, shown in Fig. 11, reveal that the spherical fullerene guest is sandwiched by two crown ether moieties with the exTTF motif serving to provide outer "flanks". In the case of both C_{60} and C_{70}, femtosecond laser flash photolysis (λ_{exc} = 480 nm, PhCN) was found to induce photoinduced electron transfer (PET) as inferred from the observation of transient species with spectral features corresponding to $exTTF^{\bullet+}$ and $C_{60}^{\bullet-}$ (or $C_{70}^{\bullet-}$). As noted by the authors, the ability to support multi-redox processes within such supramolecular ensembles could allow for the development of new artificial photosynthesis systems.

Nierengarten, Guldi, Ortí and Martín *et al*. studied a series of exTTF systems incorporating various *bis*(crown-ether) moieties, **19b–f**, with fullerene.[58,59] This systematic study revealed that the size of the crown ether played a role in regulating guest binding and served to highlight the complementary role of C–H···π interactions in the binding process as inferred from theoretical calculations (Fig. 11). Rather high binding constants were observed for the symmetrical *bis*(crown ether) derivatives [*e.g.*, log K_a(**19c**) = 4.8 ± 0.9; log K_a(**19d**) = 6.9 ± 0.2 in PhCl at 298 K]. A relatively strong interaction was also seen for the simplest of these exTTF derivatives, **19b** and C_{60} [log K_a(**19b**) = 3.3 ± 0.4]. This stands in contrast to what is seen for pristine **exTTF**, which does not significantly interact with fullerenes on its own in PhCl solution.[60] Transient absorption spectroscopic analyses revealed the formation of radical ion pairs with lifetimes ranging from 12 to 21 ps in PhCl. The energy minimised geometries of these 1:1 complexes at the B97-D/cc-pVDZ level are shown in Fig. 11.

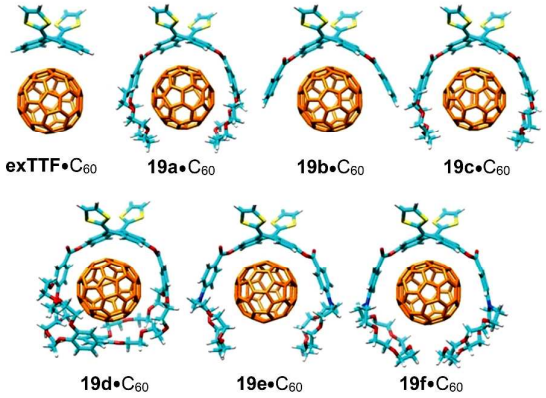

Fig. 11 Energy minimised structures of the 1:1 supramolecular complexes formed from pristine exTTF or receptors **19a–f** and fullerene. This figure is reproduced from reference 58 with permission from The Royal Society of Chemistry, copyright 2015.

A representative UV–Vis–NIR spectral titration involving **19a** with the gradual addition of C_{70} is reproduced in Fig. 12. The evolution of a broad CT-like band approximately at 580 nm was taken as evidence for formation of supramolecular complex with an empirical formula of **19a**•C_{70}.

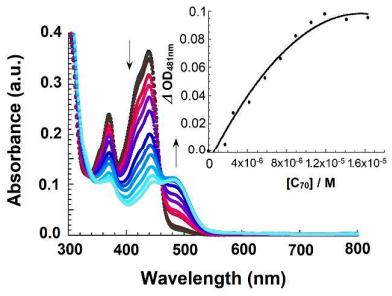

Fig. 12 UV–Vis–NIR spectra of receptor **19a** recorded upon the incremental addition of C_{70} in PhCN solution at 298 K. (Reproduced with permission from reference 57. Copyright 2010 American Chemical Society.)

4.2. ExTTF-based macrocyclic tapes. As noted above, no significant interaction between pristine **exTTF** and fullerene was seen in PhCl solution. However, increasing the number of exTTF units within a single molecular edifice transforms the system into an efficient fullerene host.[61] For instance, Martín *et al*. reported a series of macrocyclic receptors, **21–23** (Chart 5),[62,63] synthesised from the precursors **20a–b**, featuring two exTTF units that form very strong supramolecular complexes with C_{60}. At the time of publication, the largest association constant (log K_a = 6.5) was thought to be one of the highest for an all-organic C_{60} receptor system. Efforts were made by this research team to fine-tune the macrocyclic *bis*-exTTF hosts for C_{60} or C_{70} recognition through structural variations. On the basis of preliminary molecular modelling results, they explored various aromatic spacers (*e.g.*, *p*-xylene, *m*-xylene and 2,6-dimethylnaphthalene), all of which were inserted synthetically between two exTTF fragments. The exTTF subunits were further functionalised with alkene-terminated chains of different lengths and then subject to ring closing metathesis using Grubb's first generation catalyst. This allowed access to nine receptors, **21–23** (Chart 5) in a relatively straightforward synthetic manner.

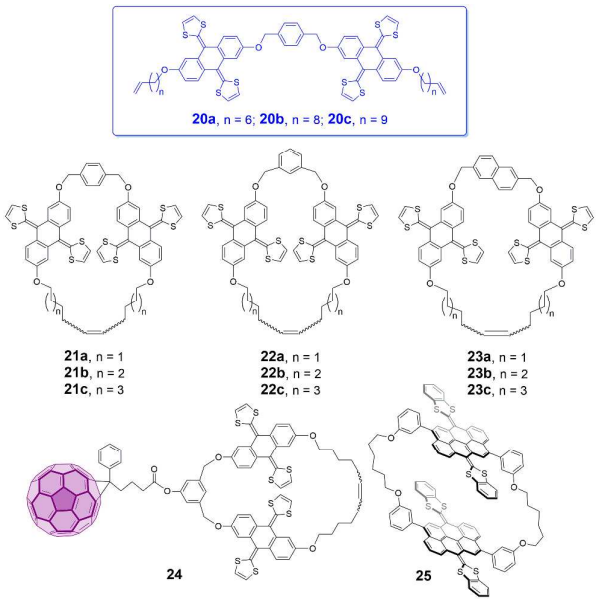

Chart 5 Chemical structures of exTTF-based macrocyclic receptors **21–25** and one series of the precursors **20a–c**.

Energy minimised (AMBER) structures of the supramolecular complexes formed between **21a–c** and C_{60} are given in Fig. 13. These theoretical studies provided further support for the claim that this class of receptors is able to encapsulate C_{60} well within their central cavities. Moreover, these theoretical studies allowed related systems, such as macrocycles **21b** and **21c** (whose sizes vary by only two methylene units), to be compared as putative fullerene (C_{60}) receptors. As the result of these geometrical optimisation studies (Figure 13), it was inferred that the slightly smaller alkenyl chain present in **21b** allows the C_{60} guest to be constrained more tightly. In fact, this system was found to bind C_{60} more effectively (log K_a = 6.5 ± 0.5 in PhCl at 298 K) than its congeners **21a,c** as determined by UV–Vis spectroscopic titrations. Job's plot experiments provide support for the conclusion that receptor **21a** forms a 1:1 complex with C_{60}, while C_{70} readily interacts with two **21a** molecules (*i.e.*, 2:1 complexation). The authors performed thorough photophysical experiments by taking all these nine *bis*-exTTF receptors, **21–23**. As an illustrative example, Fig. 14 shows the UV–Vis spectral evolution for receptors **21b**, **22b** and **23b**, respectively (one system from each series), upon the incremental addition of C_{60} in chlorobenzene (PhCl) at 298 K. In each case, a CT band centered at $\lambda_{max} \approx 425 - 430$ nm was observed along with an isosbestic point at $\approx 470 - 475$ nm. This spectral signature is thought to be due to the association of the C_{60} guest inside the *bis*-exTTF-based macrocyclic tapes. The underlying binding constant data supporting this conclusion are presented in Table 3.

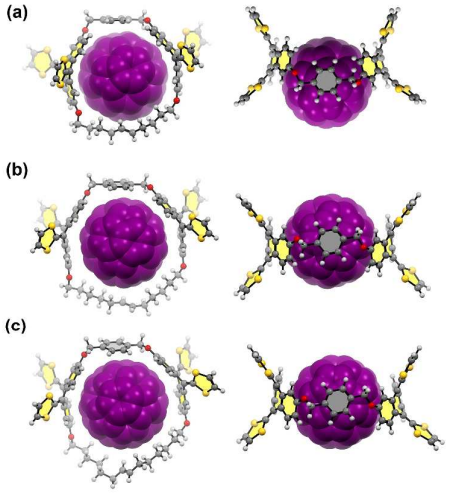

Fig. 13 Side and top views of the energy minimised structures of the supramolecular complexes (a) **21a**•C_{60}; (b) **21b**•C_{60}; and (c) **21c**•C_{60} respectively. (Reproduced with permission from reference 63. Copyright 2011 American Chemical Society.)

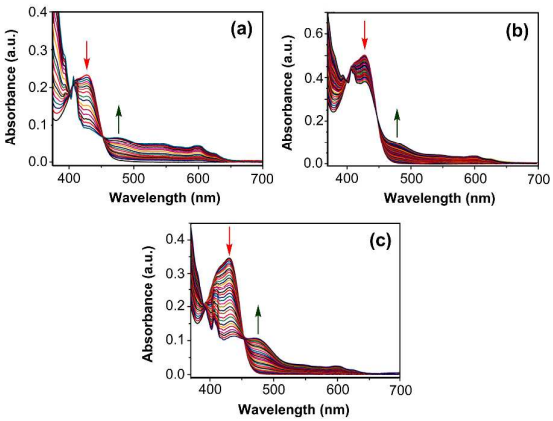

Fig. 14 Prominent UV–Vis spectral changes seen when receptor **21b**, **22b** and **23b** is titrated against C_{60} in PhCl at 298 K. (Reproduced with permission from reference 63. Copyright 2011 American Chemical Society.)

Table 3 Logarithm of the calculated binding constants for the interaction of the indicated macrocyclic hosts with C_{60} and C_{70}, as estimated from three separate UV–Vis spectral titrations carried out in PhCl at 298 K.

Comp	C_{60}	C_{70}
21a	4.3 ± 0.5	6.0 ± 0.4, 12.3 ± 0.6[a]
21b	6.5 ± 0.5	b
21c	3.5 ± 0.6	5.9 ± 0.3
22a	4.0 ± 0.5	4.4 ± 0.4; 8.3 ± 0.5[a]
22b	4.8 ± 0.4	b
22c	4.1 ± 0.4	5.4 ± 0.3
23a	4.0 ± 0.2	4.7 ± 0.3
23b	5.6 ± 0.6	5.6 ± 0.4
23c	3.4 ± 0.1	6.1 ± 0.2

[a]The first binding constant corresponds to log $K_{1:1}$ and second to log $K_{2:1}$. [b]The titration data did not allow for a satisfactory fit to a binding isotherm.

The ability of compound **24** to undergo self-assembly was demonstrated by Martín and co-workers.[64] In this study, two complementary units, *i.e.*, C_{60} and an exTTF-based macrocycle in a single molecular edifice, were found to interact with each other through presumed π–π, CT and van der Waals interactions. The monomer **24** was found to self-assemble (Fig. 15) in the gas phase, in solution and in the solid state to form linear supramolecular polymers with a very high degree of polymerisation as evidenced by large binding constant values (*log* K_a = 5.1 ± 0.5) corresponding to the individual pairwise interactions.

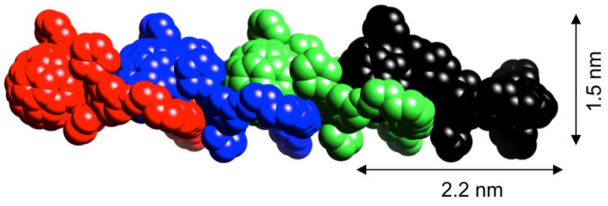

Fig. 15 Molecular mechanics (MM+) space-filling model of a tetramer of **24** showing the supramolecular self-assembled aggregation pattern. (Reproduced with permission from reference 64. Copyright 2014 Wiley-VCH Verlag GmbH & Co. KGaA, Weinheim.)

Pérez *et al*. introduced a mechanically interlocked (MINT) derivative of a single walled carbon nanotube (SWCNT) constructed by means of **21a** (*cf*. Fig. 16).[65,66] This pseudorotaxane type of molecule was synthesised *via* the ring-closing-metathesis (RCM) of two terminal alkenes within a *bis*-exTTF precursor (*e.g.*, **20a**) around the central SWCNT by means of Grubb's second-generation catalyst. Support for the proposed structure came from high-resolution scanning tunnelling electron microscopy (HR-STEM) (Fig. 16), as well as other spectroscopic means. Once formed, this MINT proved quite stable, remaining intact even after heating at reflux in tetrachloroethane (TCE) for 30 min. The authors also demonstrated that there is a substantial CT interaction between the donor exTTF moieties and the SWCNT acceptor upon photoexcitation.

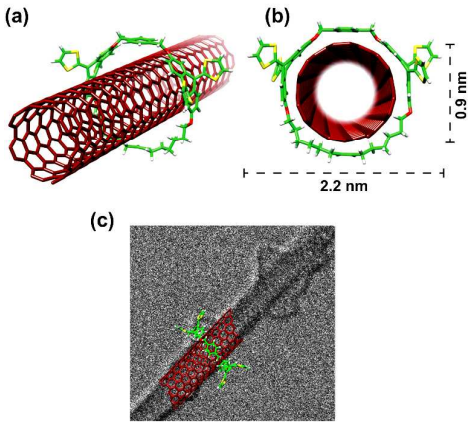

Fig. 16 (a) and (b) Energy minimised (MMFF94) molecular model of the pseudorotaxane made up from **21a** and a SWCNT; (c) HR-STEM image of the resulting MINT with the simulated molecular structures of SWCNT and *bis*-exTTF macrocycle superimposed on the image to show the proposed pseudorotaxane structure. (Reproduced with permission from reference 65. Copyright 2014 Wiley-VCH Verlag GmbH & Co. KGaA, Weinheim.)

A super-π-extended tetrathiafulvalene- (sExTTF-) based macrocyclic tape, **25**, (Chart 5) was reported[67] by Morin *et al*. This system contains two highly π-extended 9,10-*bis*(benzo-1,3-dithiol-2-ylidene)-9,10-dihydroanthanthrene moieties. As true for **24**, this receptor was found to encapsulate C_{60} well. The highly conjugated polycyclic aromatic cores present in receptor **25** allow it to act as a potential donor in forming supramolecular complexes with fullerenes. UV–Vis spectroscopic titrations involving **25** and C_{60} in toluene allowed a 1:1 association constant, $K_a = 1.2 \times 10^4$ M^{-1} to be calculated. Several related studies were carried out (*cf*. Table 4). They revealed that the binding affinities increase with increasing solvent polarity. The calculated selectivity factor $K_a(C_{70}) / K_a(C_{60})$ for **25** revealed a preference for C_{70} over C_{60}. This was ascribed to relatively more favourable interactions between the egg-shaped C_{70} than the spherical C_{60} and the aromatic polycyclic core of **25**.

Table 4 Summary of binding constants corresponding to the formation of supramolecular complexes between the sExTTF host **25** and fullerenes (C_{60} and C_{70}, respectively), as determined by UV–Vis spectroscopic titrations in toluene (PhMe) and a PhMe–MeCN solvent mixture (2:1) at 298 K.

The K_a values were calculated using a standard nonlinear least-squares fitting method and the values reported are the average of the K_a values determined from ΔA measurements carried out at 420 and 546 nm, respectively.

Solvents	$K_a(C_{60})$ (M^{-1})	$K_a(C_{70})$ (M^{-1})	$K_a(C_{70})$ / $K_a(C_{60})$
PhMe	12000	–	–
PhMe-MeCN (2:1)	43000	260000	6.0

The presumed CT band near 600 nm seen upon formation of the presumed **25**•C_{60} complex, was found to increase in intensity upon exposure to ambient light. This result was thought to reflect C_{60} sensitised photooxidation of the 1,3-dithiolylidene bonds present in **25** (Scheme 3). A light dose dependence was seen for this putative photo-oxidation process (Fig. 17).

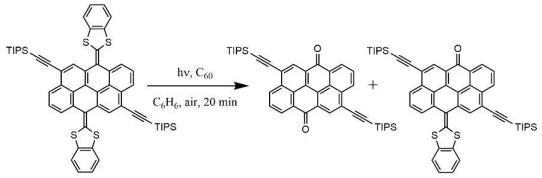

Scheme 3 Proposed visible light induced C_{60} sensitised photo-oxidation of the 1,3-dithiolylidene bonds present in the sExTTF molecular motif.

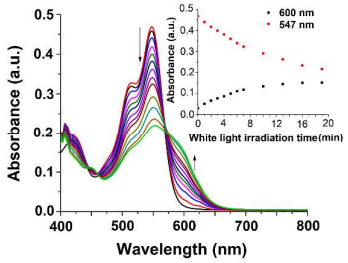

Fig. 17 Absorption spectra of a mixture of **25** (5 μM) and C_{60} (20 μM) in PhCl subject to different irradiation times. Inset: Absorbance at 600 nm (black) and 547 nm (red) vs. irradiation time. (Reproduced with permission from reference 67. Copyright 2015 American Chemical Society.)

4.3. ExTTF-based cyclotriveratrylene. Cyclotriveratrylene (CTV) derivatives (*e.g.*, **26**) are well known to form "ball and socket" complexes with spherical guests such as C_{60}.[68] de Mendoza *et al.* reported an exTTF–CTV hybrid system (**27**)[69] prepared by combining formally two different concave molecular fragments (Scheme 4). This receptor system is characterised by a preorganised bowl-shaped molecular geometry. It was found to encapsulate both C_{60} and C_{70} well. The affinity constants were found to rival the best seen for a purely organic receptor system. For instance, the log K_a values for C_{60} and C_{70} binding were found to be 5.3 ± 0.2 and 6.3 ± 0.6, respectively, in PhCl as inferred from UV–Vis spectral titrations.

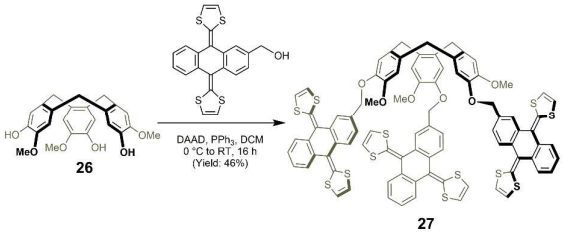

Scheme 4 Synthesis of the tripodal exTTF-cyclotriveratrylene (exTTFCTV)-based receptor, **27**.

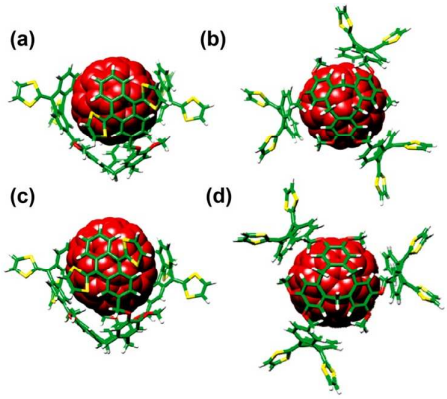

Fig. 18 Energy minimised structures of the supramolecular complexes formed from **27** and either C_{60} or C_{70}. The complexes in question have empirical formulae of **27**•C_{60} (a) side view, (b) top view; and **27**•C_{70} (c) side view, (d) top view, respectively. (Reproduced with permission from reference 69. Copyright 2010 American Chemical Society.)

Energy minimised structures inferred from DFT calculations are shown in Fig. 18. These structures provide support for the expectation that either C_{60} or C_{70} can be encapsulated within this CTV receptor. The ability of system **27** to act as receptor and sensor for fullerenes was confirmed by UV–Vis spectral titrations (Fig. 19).

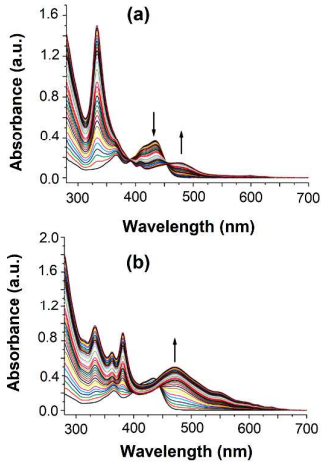

Fig. 19 UV–Vis spectral titration of compound **27** with C_{60} (a) and C_{70} (b), respectively, in PhCl at 298 K. (Reproduced with permission from reference 69. Copyright 2010 American Chemical Society.)

5. Tetrathiafulvalene vinylogues

Another class of TTF macrocycles are so-called tetrathiafulvalene vinylogues (TTFVs) represented by cyclophanes **28a,b** (Chart 6).[70] In analogy to what is true for TTF- and exTTF-based systems, TTFVs are good electron donors that are characterised by reversible electrochemical features. They also provide redox controlled structural switching behaviour that mirrors that seen for many of the exTTF systems.

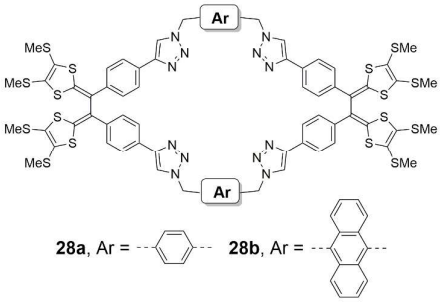

Chart 6 Chemical structures of TTFV-based cyclophanes.

These electron rich macrocycles were tested as receptors for spherical guests, such as C_{60} and C_{70}. A significant fluorescent enhancement was observed when macrocycle **28b** was treated with these fullerenes in PhCl at 298 K. This makes this system a rare example of a "turn-ON" fluorescent sensor for fullerenes. The fluorescent enhancement was thought to reflect supramolecular interactions between TTFV and fullerenes, which block PET processes that would otherwise serve to quench the fluorescence emission. Molecular modelling studies led to the suggestion that 1:2 host–guest complexes were being formed that are stabilised by interactions between the extended π-cavity of macrocycle **28b** and the fullerene guests (Fig. 20). A characteristic CT band centred at *ca.* 480 nm was observed for the resulting complexes. The intensity of this absorption band increased with increasing fullerene concentration (*cf*. Fig. 21a for studies involving C_{70}). Likewise, an increase in fluorescence intensity was seen upon the incremental addition of C_{70} as shown in Fig. 21b. Given the basic character of the TTFV moieties, the authors also evaluated the impact of protonation and found that protonation (addition of trifluoroacetic acid; TFA) could be used to engender fullerene release from cyclophane **28b**.

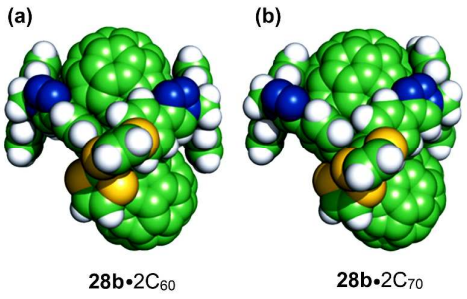

Fig. 20 CPK model of compound **28b** with C_{60} (a) and C_{70} (b), respectively, showing 1:2 host–guest binding stoichiometry. (Reproduced with permission from reference 70. Copyright 2013 American Chemical Society.)

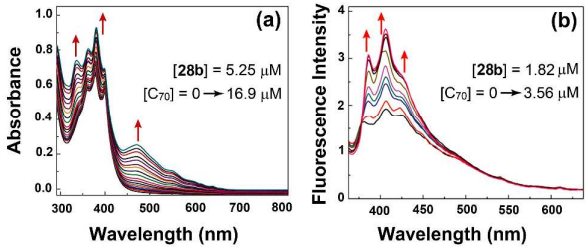

Fig. 21 Results of (a) UV–Vis spectral and (b) fluorescence titrations of compound **28b** with C_{70} in chlorobenzene at 298 K. (Reproduced with permission from reference 70. Copyright 2013 American Chemical Society.)

6. TTF-hemicarcerand and TTF-carcerands

To date only a handful of TTF-fused redox active cage systems *viz*. hemicarcerand and carcerands (Chart 7) have been reported in the literature. The systems in question have yet to be applied for any specific application. Nevertheless, their preparation sets the stage for the construction of what may emerge as the next generation of electroactive molecular receptors. Among the most aesthetically appealing of the TTF-based cage systems to be disclosed is the redox-active hemicarcerand, **29**, reported by Kaifer *et al*.[71] This cage contains four equatorial TTF subunits that serve to tether covalently two cavitand moieties. As might be expected given the presence of multiple TTF subunits, cage **29** displays multi-electron redox character. Preliminary electrochemical analyses revealed that the four TTF residues present in **29** behave independently and thus act in essence like discrete TTF molecules.

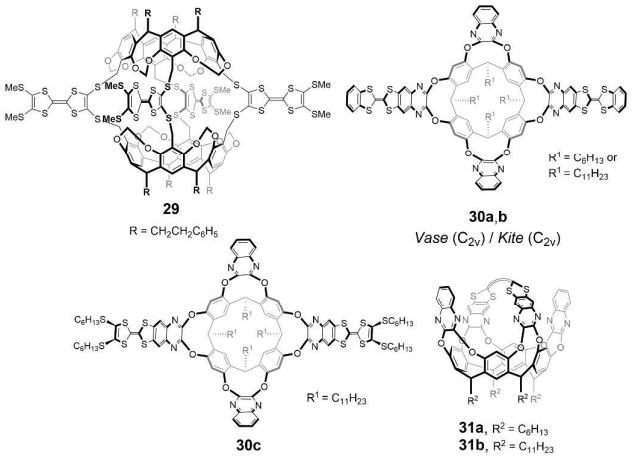

Chart 7 Chemical structures of TTF-hemicarcerand, TTF-carcerands and TTF-cavitands.

Diederich and Echegoyen *et al*. reported[72] the synthesis of the novel resorcin[4]arene-based cavitands, **30a–c**. These systems feature two extended bridges consisting of quinoxaline-fused TTF subunits. The authors found that, upon decorating both the octol bowl and the TTF cavity rims with long alkyl chains, the solubility in CH_2Cl_2 could be improved. Along with the bis-TTF cavitands **30c**, a minor amount of a novel highly strained TTF-bridged cage compound **31b** was also isolated (*cf*. Chart 7).

In the neutral form, cavitands **30a,b** were expected to adopt vase-like conformations. In contrast, upon oxidation, an open kite-like geometry was expected to dominate due to Coulombic repulsion between the two oxidised cationic TTF moieties (Scheme 5). Cyclic voltammetric (CV) and differential pulse voltammetric (DPV) analyses provided support for this proposed *vase* → *kite* conformational switching in the case of **30a**. It was proposed that this distinctive change in the form of a molecular receptor could allow for the capture a particular guest and then its subsequent release *via* simple electrochemical means. As yet, this promise has not been realised.

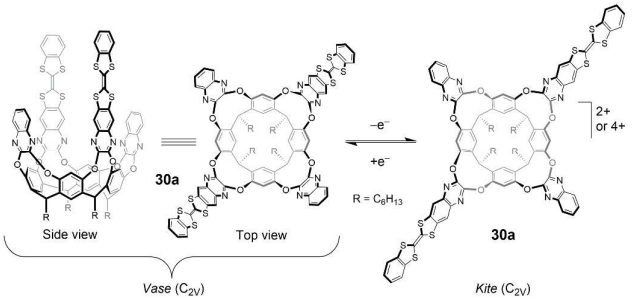

Scheme 5 The proposed redox triggered conformational switching of TTF-carcerand **30a**.

7. TTF-based calixarenes

Calix[4]arenes are another class of macrocycles that are recognised for their ability to exist in both limiting cone-like and 1,3-alternate conformations.[73–75] This is an attribute that has been specifically exploited to create hybrid calix[4]pyrrole–calix[4]arenes assemblies.[76–78] An advantage of the calix[4]arene platform relative to other macrocyclic receptor classes is that functionalisation of the upper and/or lower rims surrounding the hydrophobic cavity is straightforward. This has permitted construction of a variety of derivatives, many of which have been explored as potential receptors for various guests. A subset of these efforts has focused on combining TTF unit(s) with calix[4]arene moieties to produce compounds such as **32–44** (Chart 8) that show promise as electroactive functional materials.[79–91] The underlyting syntheses have involved either: i) Peripheral substitution of a single calix[4]arene core with either one TTF unit (*e.g*., **34**, and **37a**,**b**) or multiple TTF units (*cf*. **32a–d**, **33a–e**, **36** and **39a–c**), or ii) bridging two calix[4]arene moieties through one (*e.g*., **40a**,**b**, **41a–f**) or two (*e.g*., **35** and **38**) TTF(s) units. TTF-based thiacalix[4]arene assemblies **42a**,**b**, **43a**,**b** and **44a**,**b** have been also synthesised using similar strategies.

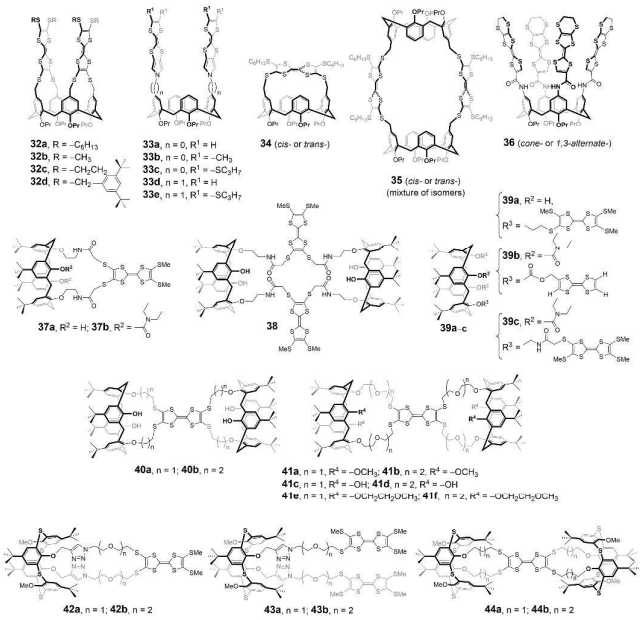

Chart 8 Chemical structures of TTF-based calixarenes.

Despite their promise, to date, only a few examples of TTF-based calix[4]arenes have been reported as being effective as receptors for either electron-deficient guests or anions. As an illustrative example, Azov *et al*. reported a molecular tweezer **33b**,[80,82] wherein two cofacial electron rich monopyrrolotetrathiafulvalenes (MPTTFs) are peripherally attached to the upper rim of calix[4]arene scaffold. Due to the quasi-parallel alignment of the two MPTTF units, **33b** is endowed with a binding site for electron deficient planar molecules. In fact, a high affinity for TCNQ was observed (K_a = 2.5 × 10^5 M^{-1} in CH_2Cl_2 at 298 K as determined by UV–Vis spectral titration). The formation of host–guest complex was evidenced by the gradual appearance of an intense CT band in the 600–900 nm spectral region. The naked eye detection of TCNQ binding was also possible since interaction leads to a visible colour change of the CH_2Cl_2 solution from light yellow to deep green. Other electron-deficient planar molecules, *e.g*., TNB and 2,4,7-trinitro-9-fluorenylidenemalononitrile (TNF) were also found to bind well to receptors **33a**,**b**.[80] Based on calculations, an intercalated structure was proposed for the host–guest complex between **33a** and TCNQ; it is shown in Fig. 22.

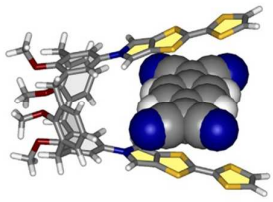

Fig. 22 Predicted structure of the supramolecular host–guest complex formed btween the TTF-calix[4]arene-based tweezer **33a** and TCNQ. Note: The –OPr groups at the lower rim of the calix[4]arene moiety in **33a** were replaced by –OMe during the calculation to reduce the cost of the

calculation. (This figure is reproduced with permission from reference 80. Copyright 2013 American Chemical Society.)

TTF subunits have also been attached to the calix[4]arene scaffold *via* secondary amide linkers to give **36**[83] and **39c**.[84] In both cases, the incorporation of TTF subunits onto the periphery of the calix[4]arene macrocyclic core produces a well-defined preorganised cavity that is able to bind test anions *via* cooperative hydrogen bonding interactions involving the secondary amide groups. Compound **36** was found to permit the electrochemical sensing of the pyrophosphate anion ($HP_2O_7^{3-}$) in CH_2Cl_2 at 298 K (Fig. 23a). It is worth noting that compound **39c** was also tested as a possible electrochemical sensor for the $H_2PO_4^-$ anion in a mixed CH_3CN - CH_2Cl_2 medium at 298 K (Fig. 23b). Contrasting electrochemical behavior was seen during the electrochemical titration of **36** and **39c** with anionic guests. In the case of $H_2PO_4^-$, a significant cathodic shift of the first TTF oxidation potential was observed when **39c** was used as a host (Fig. 23b). This shift in potentials was ascribed to the stabilisation of the anion-bound radical-cation species ($TTF^{\bullet+}$) generated by one-electron oxidation of the TTF subunit. In contrast, titrartion of **36** with $HP_2O_7^{3-}$ leads to an appreciable anodic shift ($\Delta E_{1/2}$ = 453 mV) in the first TTF redox potential (Fig 23a). This unusual behaviour was rationalized in terms of charge transfer from the propoxybenzenamine unit to the TTF moiety. This effect disappears when an anion is bound.

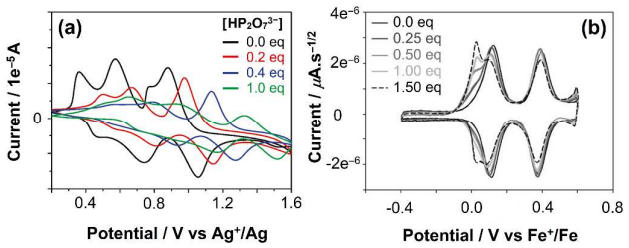

Fig. 23 a) CVs of **36** (0.5 mM in CH_2Cl_2 using $TBAPF_6$ as the supporting electrolyte and AgCl/Ag as the reference electrode) recorded upon incremental addition of $HP_2O_7^{3-}$. (Reproduced with permission from reference 83. Copyright 2010 American Chemical Society.) b) Deconvoluted CV of **39c** (0.279 mM) in CH_3CN–CH_2Cl_2, $TBAPF_6$ (0.25 M), in presence of increasing amounts of $TBAH_2PO_4$: $[H_2PO_4]$/[**39c**] = 0.00, 0.25, 0.50, 1.00, 1.50; Pt, diameter = 1.6 mm; v = 100 mV s^{-1}, vs. Fe^+/Fe. (This figure is reproduced from ref. 84 with permission from the Centre National de la Recherche Scientifique (CNRS) and The Royal Society of Chemistry, copyright 2005.)

The ability of **36** to act as an optical-based sensor was tested by UV–Vis spectroscopic means. It was found that the most significant change among the test anions studied was found in case of $HP_2O_7^{3-}$. The binding constants determined from absorption spectroscopic titrations for various anionic species in CH_2Cl_2 at 298K are summarised in Table 5.

Table 5 Calculated binding constants (K_a , M^{-1})[a] corresponding to the interactions between the cone-like and 1,3-alternate conformers of **36**, respectively, and various anions as estimated from UV–Vis spectroscopic titrations carried out in CH_2Cl_2 at 298 K.

Anions[b]	K_a, M^{-1} of receptor **36** (cone-conformer)	K_a, M^{-1} of receptor **36** (1,3-alternate conformer)
$HP_2O_7^{3-}$	4.7×10^4	9.2×10^3
$H_2PO_4^-$	3.1×10^4	5.5×10^3
F^-	2.6×10^3	1.6×10^4
Cl^-	2.8×10^3	–
$CH_3CO_2^-$	1.8×10^4	9.5×10^3

[a]The estimated errors are <20%. [b]Anions were used in the form of their tetrabutylammonium (TBA) salts. [c]No reliable fit was obtained; presumably, this is due to the formation of a mixture of 1:1 and 1:2 complexes.

Sallé and co-workers reported[84–90] a series of calix[4]arene-based molecular systems (**37a**,**b**, **38**, **39a–c**, **40a**,**b** and **41a–f**) bearing pendant TTF units attached to the upper rim of a calixarene core. The design strategy of these macromolecules is based on the combination of three distinct components in a single molecular scaffold, *viz*. a calix[4]arene moiety (to define the spatial organisation), flexible polyethers or amide functionalities (to provide a 3D binding site for alkali metals), and electroactive TTF transducers (to allow the putative complexation events to be monitored by electrochemical means).

Compound **39b** was found to form dimeric $[(TTF)_2]^{\bullet+}$ and $(TTF^{\bullet+})_2$ species that could be disassociated upon Na^+ binding.[87] Specifically the dimerisation process was thought to be inhibited by the recognition of the cation within the 3D pocket created by the four neighbouring ester groups present in **39b**. On the basis of a single crystal structure of the Na^+ complex of **39b** (shown in Fig. 24), it is suggested that metal complexation to the lower rim of the calix[4]arene core leadis to a splaying out of two TTF units that, in turn, inhibits strong inter-complex interactions.

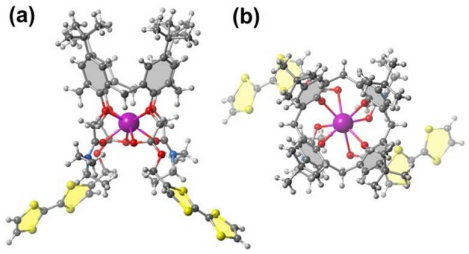

Fig. 24 Single crystal X-ray structure of the Na^+-complex of **39b**; (a) side view and (b) view from the top. Solvent molecules and anions are omitted for clarity. (This figure was redrawn using data that were originally published in references 87.)

Sallé *et al*. used a series of *bis*(calix[4]crown)tetrathiafulvalene receptor systems, **41a–f**, to detect metal ions electrochemically.[88,90] Single crystal X-ray diffraction analyses (*cf*. Figure 25) provided

support for the notion that the metal ion (*e.g.*, Na^+) is coordinated within the pockets formed at the lower rim of each calix-crown moiety.

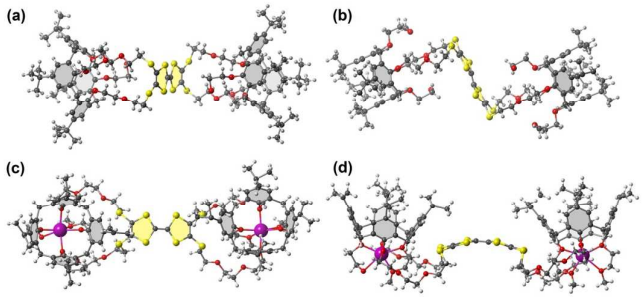

Fig. 25 (a) and (b): Two views of the single crystal X-ray structure of the free receptor **41e**. (c) and (d): Binding mode seen for the Na^+ cation complex of the calix[4]crown receptor **41f**. Solvent molecules and anions are omitted for clarity. (This figure was redrawn using data that were originally published in reference 88.)

The TTF-functionalised thiacalix[4]arenes, **42a**,**b**, **43a**,**b** and **44** (*cf*. Chart 8) were also reported recently.[91] These molecules were used to study metal ion-induced intermolecular ET processes in the presence of an electron poor tetrachlorobenzoquinone (TCNQ) guest in a 1:1 mixture of MeCN–CH_2Cl_2 at 298 K. In the presence of metal ions, compounds **43a**,**b** show more efficient ET as compare to **42a,b**, a finding that was ratioinalized in terms of the presence of an extra TTF unit in **43a**,**b**, which enhances the interactions between the oxidized TTF ($TTF^{\bullet+}$) and the tetrachlorobenzoquinone radical anion ($TCNQ^{\bullet-}$).

8. TTF-based cages and cryptands

Cryptands are classic three dimensional macrobicyclic molecular motifs that have been exploited for a range of ion binding applications. By incorporating TTF motifs into cryptand-like structures, a variety of systems can be synthesised that could serve as electroactive host–guest receptors. With such considerations presumably in mind, a series of TTF-based cages and cryptands, **45**–**47**, (Chart 9) with various spacers at the apical positions, were designed and synthesised by Becher *et al*.[92] These molecular cages contain three individual TTF-bridges connected to apical tripodal motifs; they were prepared using a high dilution strategy that involved the selective protection-deprotection of precursor TTF-thiolates.

A pyrrolo-TTF three dimensional belt (**48**) was also reported[93] by Becher *et al*. The ability of this system to bind TCNQ was investigated in solution using UV–Vis, ^{1}H NMR and electron paramagnetic resonance (EPR) spectroscopies. It was observed that when 1 equiv. of TCNQ was added to a CH_2Cl_2 solution of **48** (2.5×10^{-4} M) an instantaneous visual colour change from orange to green was observed on the laboratory time scale. The appearance of two bands, centred at λ_{max} 749 and 849 nm, respectively, in the UV–Vis spectrum (Fig. 26) was thought to reflect a transfer of charge between **48** and the bound TCNQ guest. Neither **48** nor TCNQ absorbs appreciably beyond 600 nm. EPR spectroscopic analyses of **48**•TCNQ recorded in CH_2Cl_2 revealed a radical signal at g = 2.009. The line width and g-value are consistent with the presence of a $TTF^{\bullet+}$. These results thus support the assumption that charge transfer between the host and guest takes place in solution. That two CT bands were seen was ascribed to the possible presence of two different supramolecular binding modes in solution, namely, an inside and an outside (alongside) binding mode. However, a solid state X-ray crystal structure analysis of the CT complex **48**•TCNQ revealed that in the solid state the TCNQ is associated outside of receptor **48** (Fig. 27) adopting a slipped sandwiched structure.

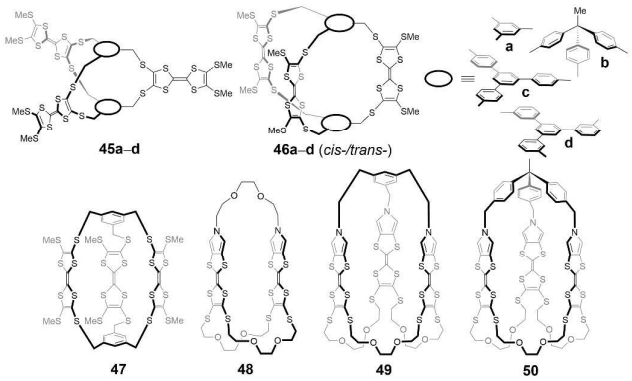

Chart 9 Chemical structures of TTF-based cages and cryptands.

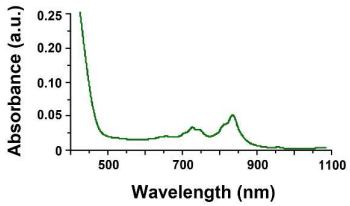

Fig. 26 Absorption spectrum of **48** recorded in CH_2Cl_2 in the presence of TCNQ. (Reproduced with permission from reference 93. Copyright 2002 American Chemical Society.)

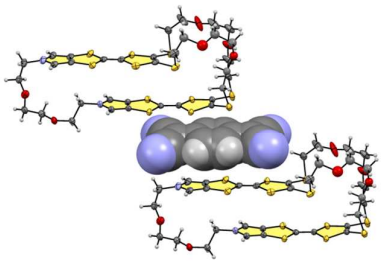

Fig. 27 Solid state X-ray structure of the outside binding mode complex formed from **48** and TCNQ. Residual solvent molecules are omitted for clarity. This figure was redrawn using data that were originally published in reference 93.

Two novel TTF-cages, **49** and **50**, containing three monopyrrolo-TTF (MPTTF) units were reported[94,95] by Jeppesen and co-workers. A

single crystal X-ray diffraction analysis (Fig. 28a) revealed that **49** is able to accommodate only solvent molecules ($CDCl_3$) as guests within its cavity. The system was thus considered too small to act as a receptor for larger substrates. Replacing the triethylbenzene "lid" of cage **49** by a larger triarylethane "roof" led to cage **50**, which was considered appropriately sized to recognise C_{60}. The formation of a strong 1:1 donor–acceptor (D–A) complex C_{60}⊂**50** was confirmed by a solid state X-ray diffraction analysis (Fig. 28c), as well as by shifts in the ^{1}H NMR and UV–Vis absorption spectroscopic features. A prominent CT band (λ = 735 nm, $\varepsilon \approx 840$ M^{-1} cm^{-1}) was observed when 1 molar equiv. of C_{60} was added to a CH_2Cl_2 solution of **50** (Fig. 29, brown line). Replacing C_{60} by $Li^+@C_{60}$ led to a *ca*. 28-fold increase in the binding affinity ($K_a = 3.7 \times 10^6$ M^{-1} vs. $1.3 \pm 0.6 \times 10^5$ M^{-1} in CH_2Cl_2) and gave rise to a large bathochromic shift in the CT band (λ = 1104 nm, $\varepsilon \approx 4800$ M^{-1} cm^{-1}). The greater affinity seen for $Li^+@C_{60}$ was rationalised in terms of enhanced coulombic interactions relative to C_{60} within the corresponding complexes, $Li^+@C_{60}$⊂**50** vs. C_{60}⊂**50**. PET was also seen upon photoexcitation of $Li^+@C_{60}$⊂**50**; this was not observed for C_{60}⊂**50**.

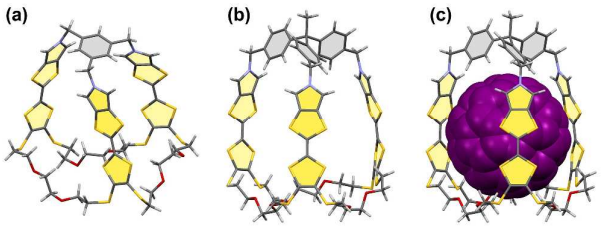

Fig. 28 Crystal structures of the TTF-based cages **49** (a) and **50** (b), respectively. The C_{60} molecule is deleted from the structure of the complex formed with **50** to show that it possesses a larger cavity than **49**. (c) View of the single crystal X-ray structure of C_{60}⊂**50**. Residual solvent molecules have been omitted for clarity. This figure was redrawn using data that were originally published in references 94 and 95.

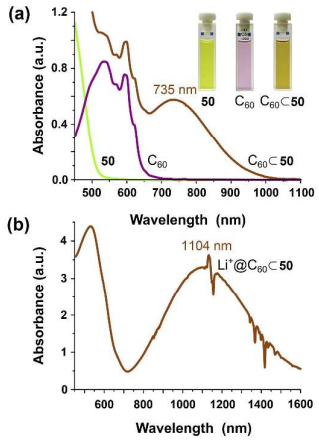

Fig. 29 (a) Vis–NIR spectra of TTF-based cage **50**, C_{60}, and their supramolecular complex **50**•C_{60}, respectively, as recorded in CH_2Cl_2 at 298 K; (Note that the CT band is centred at 735 nm). (b) Vis–NIR spectra of the supramolecular complex formed by cage **50** and $Li^+@C_{60}$ in CH_2Cl_2 at 298 K. In this case, the CT band is centred at 1104 nm. (This figure is reproduced with permission from reference 95, with permission from The Royal Society of Chemistry, copyright 2017.).

9. TTF- and exTTF- based metalla-macrocycles and cages

The use of coordination driven self-assembly has allowed chemists to synthesise *inter alia* a range of sophisticated molecular polygons. In certain cases, this can be done in a single step and in high yield.[96–100] For many applications, the design of stimuli-responsive receptors is critical. With such considerations in mind, Sallé, Goeb and co-workers have been working to prepare self-assembled metalla-cages based on TTF-containing ligands. Particular emphasis has been devoted to the use of precursors based on the bis(pyrrolo)TTF (BPTTF) derivatives, (**51, 52**), TTF-based tetrapyridyl ligand, **53** and 9,10-bis(1,3-dithiol-2-ylidene)-9,10-dihydroanthracene (exTTF) motifs (**54**–**56**) (Chart 10).

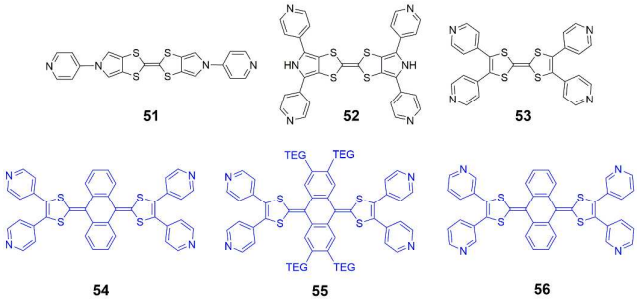

Chart 10 Chemical structures of various BPTTF-, TTF- and exTTF-derived ligands.

9.1. BPTTF-based metalla-macrocycles and cages. An efficient way to generate metalla-macrocycles involves the use of a rigid linear ligand (*e.g.*, 4,4'-bipyridine) in conjunction with a square-planar *cis*-blocked metal (M) complex (*e.g.*, with M = Pd^{2+} or Pt^{2+}) in accord with the procedures pioneered by Fujita[101] and Stang.[102] Such an association is likely to produce a molecular square. Nevertheless, complexation-based self-assembly is often accompanied by the formation of entropically favourable triangular homologues, in particular, when the ligand is either elongated or not sufficiently rigid.[103,104]

When the *cis*-blocked square planar Pt(*dppp*)$(OTf)_2$ complex [*dppp* = 1,3-*bis*(diphenylphosphino)propane] was treated with the rigid rod shaped BPTTF ligand (**51**), a self-assembled molecular triangle (**57**) and a molecular square (**58**) were produced (Scheme 6) in 60% and 31% yields, respectively.[105,106]

Cyclic voltammetry (CV) analyses revealed that, as true for the isolated parent BPTTF unit, each BPTTF unit in **57** and **58** can be independently oxidised *via* two successive reversible oxidation steps. Therefore, it is possible to generate in a controlled way species with six and eight positive charges directly on the cavity panels in the case of **57** and **58**, respectively.

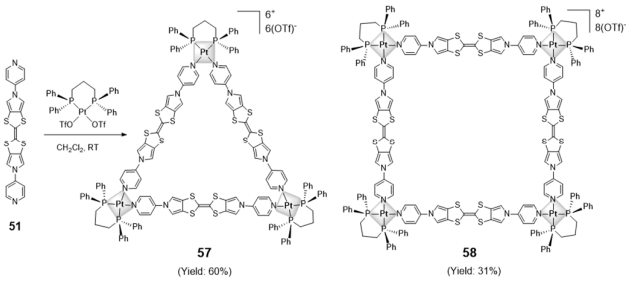

Scheme 6 Synthesis of an electron-rich BPTTF molecular triangle and the corresponding square.

Among these two self-assembled polygons, the triangular analogue **57** was considered appropriately sized to encapsulate C_{60} (cavity diameter = 13 Å). The ability of **57** to interact with C_{60} was monitored by means of UV–Vis spectroscopic titrations. This allowed a binding constant of log K_a = 4.2 M^{-1} (CS_2/CH_2Cl_2: 8/2 v/v) to be calculated as determined using the Benesi-Hildebrand equation for a 1:1 complexation event. This ability to bind C_{60} was ascribed to the combined effect of van der Waals and π–π interactions, as well as the preorganised nature of the host. It is worth noting that no appreciable binding of C_{60} was seen in the case of the larger homologue, *i.e.*, square **58**.

The BPTTF molecular skeleton was functionalised in the α positions of the pyrrole ring to produce the tetratopic ligand **52**. When this latter ligand was allowed to react with a *cis*-coordinated square-planar Pt(II) complex (*cf*. Scheme 7), a three dimensional polycationic metalla-cage **59** was produced.[107,108] A ^{1}H DOSY NMR spectroscopic study was carried out and provided support for the conclusion that only a single discrete ensemble was formed as the result of this reaction.

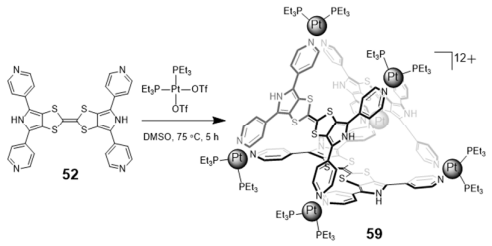

Scheme 7 Synthesis of the electron rich BPTTF-based, Pt^{2+}- trigonal prismatic cage, **59** from its tetratopic precursor **52**.

CV studies revealed two successive oxidation processes. This was taken as evidence that the three redox active BPTTF units that make up the panels of **59** act in an electrochemically independent way. The potentials are shifted anodically relative to those of the parent BPTTF unit (for **59**: E^1_{ox} = +0.43 V and E^2_{ox} = +0.62 V vs. Fc/Fc^+; for BPTTF: E^1_{ox} = –0.02 V and E^2_{ox} = +0.23 V vs. Fc/Fc^+ in DMF, using 0.1M NBu_4PF_6 as the electrolyte). These shifts were attributed to a combination of electronic and structural effects: i) Metal coordination serves to decrease the donor character of the BPTTF core and ii) this effect is amplified by the co-planarity between the pyridine coordinating groups and the BPTTF backbone. Evidence for this latter co-planarity came from a solid state single-crystal X-ray diffraction analysis of **59** (Fig. 30), which also served to confirm its overall structure.

The trigonal prismatic structure found in the solid state led the Angers research group to explore the possibility of using **59** to encapsulate electron deficient guests. Particular success was encountered in the case of tetrafluorotetracyano-*p*-quinodimethane (F_4TCNQ), which was found to form a 1:1 adduct with **59** as evidenced by a Job plot analysis involving UV–Vis spectroscopic titrations.[107] When **59** was titrated with F_4TCNQ, new absorption bands appeared that were attributed to formation of $F_4TCNQ^{\bullet-}$ and $BPTTF^{\bullet+}$ radical species. The driving force for complex formation was thus ascribed D–A type π–π interactions between the BPTTF host and the F_4TCNQ guest.

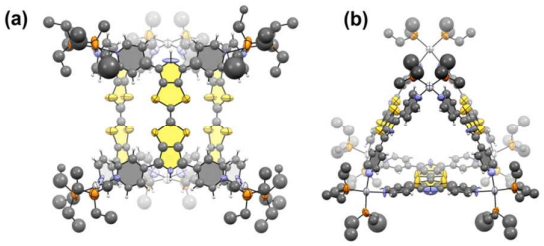

Fig. 30 X-ray crystal structure of the electroactive metalla-cage **59** (a) side view; (b) top view. Residual solvent molecules have been omitted for clarity. This figure was redrawn using data that were originally published in reference 107.

9.2. TTF-based metalla-cages. In an effort to prepare additional metalla-rings and cages containing the TTF subunit, the tetrapyridyl ligand **53** was synthesised. An X-ray diffraction analysis of **53** revealed that the four pyridine nitrogen atoms define a rectangle of 6.7 × 13.1 Å (Scheme 8).[109] However, two pyridyl units are rotated with respect to the TTF plane. This is thought to result in a moderate delocalisation of π-electron density between the electron-rich TTF unit and the electron-withdrawing pyridine motifs present in **53**. Nevertheless, the π-donating character of the constituent TTF unit was expected to be largely preserved in the case of **53**, in contrast to what was expected for the tetrapyridyl-BPTTF ligand **52**.

Ligand **53** reacts with *cis*-M(*dppf*)$(OTf)_2$ complexes (M = Pt^{2+} or Pd^{2+}; *dppf* = 1,1′-*bis*(diphenylphosphino)ferrocene; OTf = trifluoromethane-sulfonate) to afford large self-assembled electroactive M_8L_4 type metalla-cycles, **60a,b** (Scheme 8).[109] The electrochemical properties of these two representative systems, **60a** and **60b**, were compared with those of ligand **53** by means of cyclic voltammetric analyses (Fig. 31).

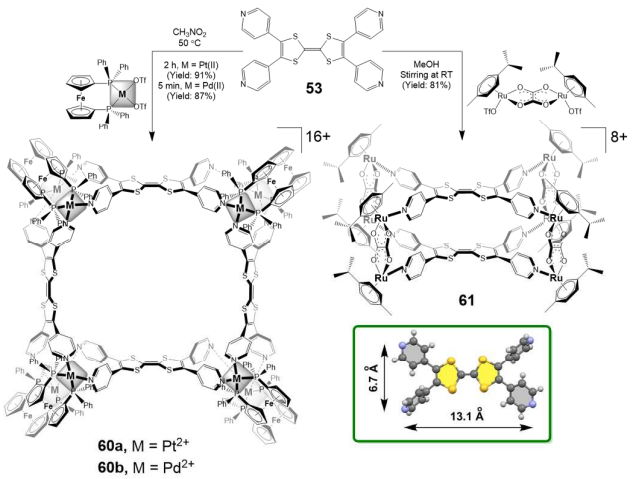

Scheme 8 Synthesis of self-assembled TTF-containing metalla-cages **60a,b** and **61**, respectively. Inset: Single crystal X-ray diffraction structure of the tetradentate ligand **53**.

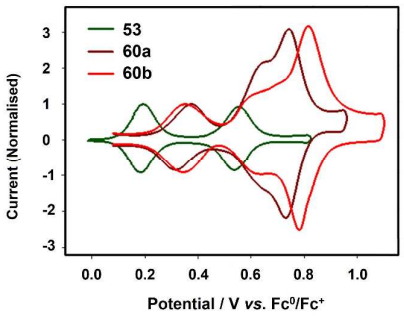

Fig. 31 Deconvoluted cyclic voltammograms of ligand **53** (C = 10^{-3} M, CH_3CN/CH_2Cl_2, 0.1 M *n*-Bu_4NPF_6, 100 mV s^{-1}), and of squares **60a** and **60b** (C = 5×10^{-4} M, CH_3CN, 0.1 M *n*-Bu_4PF_6, 20 mV s^{-1}), using a carbon graphite working electrode, V vs. Fc^0/Fc^+. (This figure was reproduced from reference 109.)

As compared to the oxidation potentials of free ligand **53**, after metal complexation, a slight positive shift (*e.g.*, for **60a**, ΔE^1_{ox} = +0.16 V and ΔE^2_{ox} = +0.10 V in CH_3CN/CH_2Cl_2) was seen in the redox wave ascribed to the TTF unit. A third reversible oxidation wave was observed at a higher potential, which corresponds to the simultaneous oxidation of the eight ferrocene units (*dppf*) situated at corner of the cage. Therefore, based on these data it is possible to tune the global charge of cages **60a,b** electrochemically, over a remarkably wide window, namely from species bearing 16 to 24 positive charges. The same TTF-based ligand **53** was also found to undergo self-assembly when treated with dinuclear *p*-cymene ruthenium complexes.[110] In particular, the metalla-cage **61** could be produced. In this system the presence of two cofacial TTF units limits the size of the cavity and no evidence of guest binding was seen.

9.3. ExTTF-based metalla-cages. Due to its unique structural and electronic properties, 9,10-*bis*(1,3-dithiol-2-ylidene)-9,10-dihydroanthracene (exTTF) has attracted attention recently.[15,111–113] Although, exTTF adopts a butterfly shape in its neutral state, presumably as the result of 1,5-interactions between the S atoms of the 1,3-dithiolylidene moieties and the periplanar dihydroanthracene hydrogen atoms, its corresponding dicationic species displays two aromatic 1,3-dithiolium rings connected to the central aromatic anthracene moiety. The latter state can be accessed *via* a two-electron oxidation process. This oxidation is characterised by a single pseudo-reversible oxidation wave, located at E_{ox} = –0.04 V (vs. Fc/Fc^+), under conditions of cyclic voltammetry. However, a lack of electrochemical reversibility is usually seen, a finding ascribed to the drastic conformational change that occurs upon oxidation. These features prompted efforts to incorporate the exTTF subunit into metalla-cages. With such a goal in mind, Goeb, Sallé and co-workers reported a series of self-assembled metalla-macrocyclic molecular receptors constructed from the redox active exTTF tetrapyridyl ligands **54** and **55** (Scheme 9).[114–118]

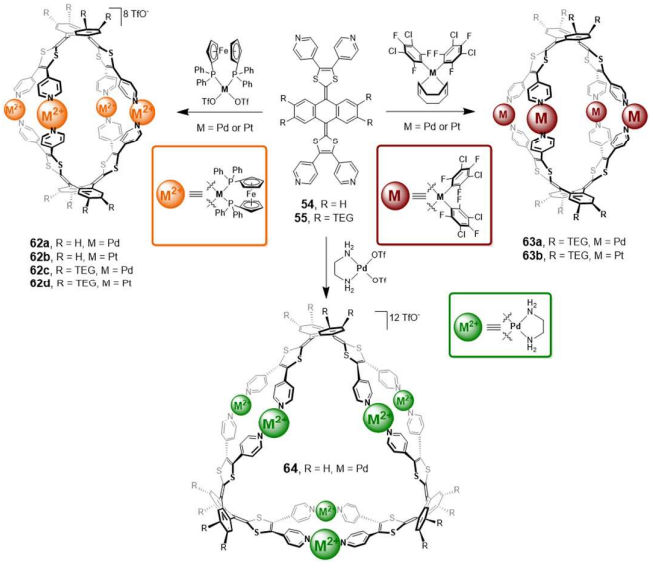

Scheme 9 M_4L_2 type (**62a–d** and **63a,b**) and M_6L_3 type (**64**) metalla-macrocyclic molecular receptors constructed from the redox active exTTF ligands **54** and **55**. TEG: triethylene glycol monomethyl ether.

Reaction of ligand **54** with *cis*-M(*dppf*)$(OTf)_2$ (where, M = Pd^{2+} or Pt^{2+}) complexes (Scheme 9 and Fig. 32) produced the large metalla-macrocyclic $M_4L_2^{8+}$ systems **62a,b**, in which the internal cavity is bridged by two concave redox active electron donating exTTF units.[114] Container **62a** and **62b** allowed for the complexation of one perylene guest with 1:1 binding stoichiometries $K_a = 3.9 \times 10^3$ M^{-1} and 3.2×10^3 M^{-1}, respectively, in CD_3NO_2 as determined from ^{1}H DOSY NMR spectroscopic titrations.

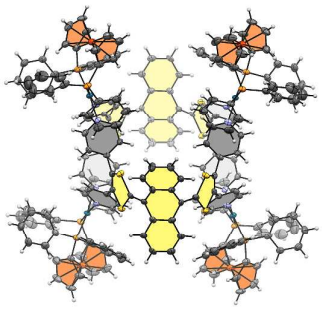

62a, when M = Pd^{2+}

Fig. 32 Solid state structure of polycationic exTTF-based metalla-macrocycle **62a** (M = Pd^{2+}). This figure was redrawn using data that was originally published in references 114.

Efforts to produce similar self-assembled metalla-cages using the *cis*-blocked complex Pd(*en*)$(NO_3)_2$ [where, *en* = ethylenediamine] likewise afforded one unique discrete compound (**64**).[116] Complex **64** was considered to be larger than **62a,b** as inferred from the diffusion coefficient measured by ^{1}H DOSY NMR spectroscopy. A solid state structural analysis of **64** (Fig. 33a) provided support for the formation of a self-assembled system with a generalised empirical formula of $M_6L_3^{12+}$. The fact that different discrete metalla-cage species are formed under similar conditions serves to underscore the crucial role of the metal complex, and in particular the metal co-ligand, plays in directing the self-assembly process (Figs. 33b,c).

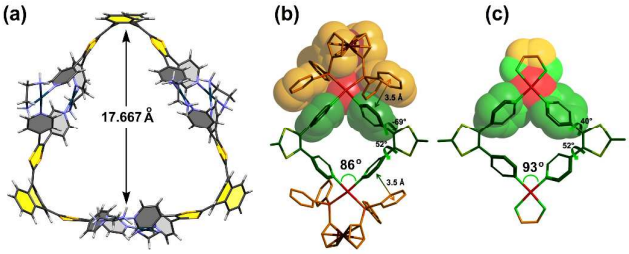

Fig. 33 (a) X-ray structure (SOLEIL synchrotron) of exTTF-based trigonal cage **64**; (b) geometry around the metal cation (Pd^{2+} centre) in **62a** and (c) geometry around the metal cation (Pd^{2+} centre) in **64**. The exTTF moieties are not shown for the sake of clarity in panels (b) and (c). (This figure was reproduced from reference 116.)

The Sallé group also designed ligand **55**, which incorporates four triethylene glycol monomethyl ether (TEG) chains. This functionalisation offers advantages in terms of forming metalla-cages: i) The TEG chains result in a higher solubility, which allows a greater range of experimental conditions to be explored in the context of self-assembly and facilitates host–guest studies and ii) the π-donor character of the ligand and of the corresponding cage cavity is increased as the result of a donating mesomeric effect promoted by the oxygen atoms directly linked to the dihydroanthracene skeleton. Ligand **55** self-assembles (Scheme 9) in the same way as **54** in the presence of *cis*-Pd(*dppf*)$(OTf)_2$ to afford the $M_4L_2^{8+}$ cage **62c** in near-quantitative yield.[115] The cavity of **62c** is similar in size to that of **62a**, and so is its ability to bind flat polyaromatic species. As expected for a system bearing pendant TEG groups, oxidation of both ligand **55** and cage **62c** occurs at lower potentials than for the homologous ligand **54** and analogous cage **62a**, respectively. As a result of the rather unique combination of electronic and conformational features of framework, **62c** (*i.e.*, good π-donating ability and drastic conformational changes that occur upon oxidation), reversible disassembly-reassembly of the redox-active cavity is observed upon successive chemical oxidation and reduction.

Of interest is that the positively charged Pd^{2+} centres are located on the "equator" of the ovoid cavity. Therefore, it is considered likely that these charges can contribute directly to the binding of anionic species. In the case of the large and spherical dodecafluorododecaborate anion ($B_{12}F_{12}^{2-}$), evidence in support of this notion came from ^{19}F DOSY NMR experiments carried out in CD_3CN solution and solid state X-ray diffraction analyses (Figs. 34a,b). Remarkably, the reversible redox-triggered disassembly noted in the case of the free cage **62c**, could also be effected in the case of the $(B_{12}F_{12}^{2-})_2\subset$**62c** host–guest complex. This system might thus offer a new option for the redox-based binding and controlled release of guests.

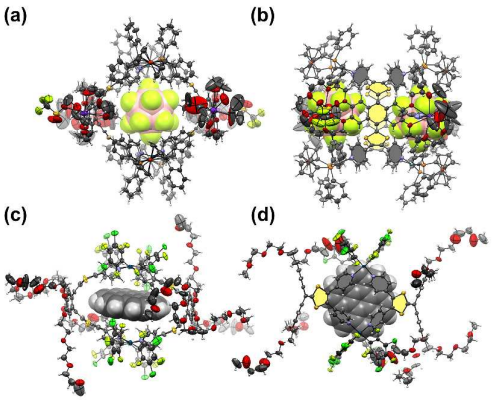

Fig. 34 Single crystal X-ray diffraction structures of two host–guest complexes prepared from cages **62c** and **63a**, respectively: (a) top view and (b) side view of the complex $(B_{12}F_{12}^{2-})_2\subset$**62c**. Residual solvent molecules are omitted for clarity. (c) Top and (d) side views of the complex coronene$\subset$**63a**. This figure was redrawn using data that were originally published in references 115 and 117.

An important issue in host–guest chemistry concerns the binding of neutral guests. Typically, this presents a greater challenge than the recognition of ionic species due to the inherent lack of coulombic interactions. Metalla-cages obtained through the coordination-driven self-assembly are predominantly polycationic species. This and the presence of coordinated counter anions can limit the ability of such species to act as receptors for neutral guests. In contrast, were they available, neutral metalla-cages might allow for the binding of non-charged substrates. Efforts were thus

made to obtain neutral metalla-cages containing TTF subunits. By using specific Pd^{2+} or Pt^{2+}-complexes, *i.e.*, *cis*-M(*dctfb*)$_2$(*cod*), where, M = Pd^{2+} or Pt^{2+}, *dctfb* = dichlorotrifluorobenzene and *cod* = cyclooctadiene, in conjunction with the tetrapyridyl ligand, **55**, (Scheme 9), it proved possible to obtain the neutral M_4L_2 cages **63a** and **63b**, respectively. Both systems were characterised in the solid state by single crystal X-ray diffraction analysis (see Fig. 35 for a view of the solid state structure of **63a**).[117]

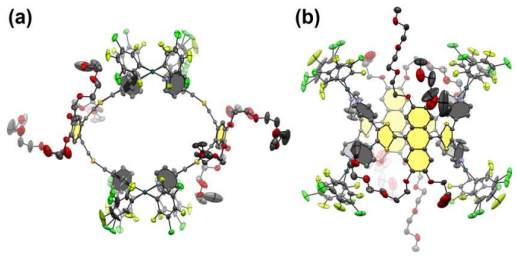

Fig. 35 Single crystal X-ray structures of the neutral M_4L_2 cage **63a**. Views from top (a) and (b) side. Residual solvent molecules are omitted for clarity. This figure was redrawn using data that were originally published in reference 117.

While showing similar geometries and dimensions as the polycationic cages **62c** and **62d**, the neutral cages **63a** and **63b** differ by the absence of counter anions. This matched set thus offered a unique opportunity to compare the binding ability of ostensibly similar cages that differ only by the overall charge. A comparative binding study involving the polycationic cage **62c** and neutral cage **63a** and various neutral polyaromatic hydrocarbons was performed by means of ^{1}H DOSY NMR spectral analyses carried out in either a 4:1 or 1:1 mixture of CD_3NO_2 and $CDCl_3$ at 298 K. This study revealed that the neutral hosts were much more effective receptors for these substrates under these experimental conditions (Table 6).

Table 6 Calculated binding constants K_a for cationic cage **62c** and neutral cage **63a** towards various planar polyaromatic guests as estimated from ^{1}H DOSY NMR spectroscopic studies carried out in either 4:1 or 1:1 mixtures of CD_3NO_2 and $CDCl_3$ at 298 K (C = 2 × 10^{-3} M).

Guests	Solvent CD_3NO_2:$CDCl_3$	$M_4L_2^{8+}$	M_4L_2 (Neutral)
Coronene	4:1	170[a]	1.1×10^5
Coronene	1:1	63	2.6×10^6
Perylene	1:1	96	4.0×10^7
Triphenylene	1:1	14	2.8×10^2
Pyrene	1:1	b	1.7×10^2

[a]The cage concentration (C) = 10^{-3} M during these experiments. [b]No significant guest binding was detected under the experimental condition.

The electrochemical properties of the neutral cages **63a,b** were studied and compared with those of ligand **55** (Fig. 36).[118] As expected given the presence of coordinated metal centres, higher oxidation potentials are seen for the cages (*e.g.*, $\Delta E_{ox} \approx +0.28$ V ≈ + 0.31 V relative to **55** in case of **63a** and **63b**, respectively). Nevertheless, oxidation still occurs readily.

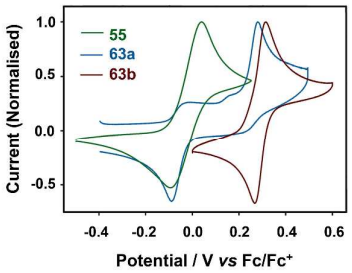

Fig. 36 Cyclic voltammograms of ligand **55**, cages **63a** and **63b** (the cage concentration (C) was fixed at 10^{-4} M, CH_3CN/CH_2Cl_2, 0.1 M *n*-Bu_4NPF_6, 100 mV s^{-1}, carbon graphite working electrode) V vs. Fc/Fc^+. (Reproduced with permission from reference 118. Copyright 2017 Wiley-VCH Verlag GmbH & Co. KGaA, Weinheim.)

The electrochemical behaviour of the palladium cage (**63a**) and of the platinum cage (**63b**) differs from one another. Whereas, an electrochemically irreversible oxidation of the exTTF derivatives was observed for cage **63a**, the platinum analogue (**63b**) exhibits a quasi-reversible oxidation wave. On this basis, it was inferred that in contrast to **63b**, little cage disassembly takes place upon oxidation of the neutral platinum cage (**63a**). The greater stability seen in the case of **63b** is attributed to the relatively more robust nature of the pyridine-platinum coordination bond. In purely operational terms this difference means that with **63b** it is possible to generate reversibly *via* oxidation species with up to four positive charges without destroying the assembly.

The neutral platinum cage **63b** was found to act as an effective receptor for coronene, producing an overall neutral 1:1 complex as inferred from ^{1}H NMR, FTIR, HRMS and fluorescence spectroscopic studies. Comparative spectroelectrochemical analyses revealed that coronene binding and its electrochemical complexation-expulsion depends on the overall charge state on the cage. This led to the suggestion that the coronene is displaced from the receptor by one or more anions once the host is oxidised. Support for this conclusion came from DFT calculations.[118]

10. TTF-based metal-organic-frameworks (MOFs) and covalent-organic-frameworks (COFs)

10.1. TTF-based MOFs. Metal–ligand coordination strategy also provides another promising approach to construct self-assembled three dimensional (3D) architectures. These are not discrete macrocyclic systems or cages as discussed earlier. However, they create infinite cavities (or channel) within the 3D network, which make these materials of potential interest in the context of many

applications, *e.g*., gas storage, catalysis, guest separation *etc*. In fact, several examples of 3D MOFs based on TTF-functionalised multidentate ligands have been reported in recent years.[119–125] TTF-based building blocks commonly used for this purpose contain either pyridine or carboxylates as metal coordinating sites. Two tetratopic ligands based on TTF tetracarboxylates are shown in Chart 11. A recent review[125] has highlighted various TTF-based coordination polymers and discussed their potential applications. However, a brief summary from the perspective of the TTF synthetic chemist is deemed appropriate here.

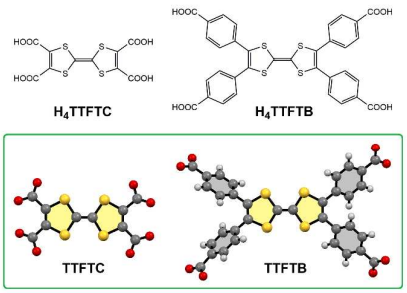

Chart 11 Chemical structures of TTF-tetracarboxylic acid precursors commonly used for making MOFs. Inset: Crystal structures of their corresponding TTF-tetracarboxylate building blocks.

Some of these TTF-containing MOF materials were demonstrated to act as functional materials with interesting electronic and magnetic properties. For example, Dincă *et al*. reported porous and conductive 3D MOFs (Fig. 37) based on the tetratopic ligand TTFTB that proved capable of efficient "through-space" intrinsic charge transport.[120,121]

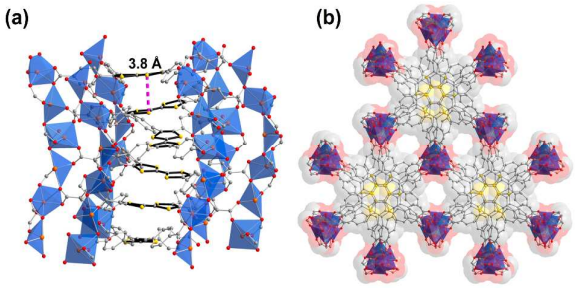

Fig. 37 (a) Side view of the infinite helical stack of TTF moieties that are present within the MOF produced from H_4TTFTB in 3:1 DMF/EtOH, and $Zn(NO_3)_2 \bullet xH_2O$ in 1:1 EtOH/H_2O (75 °C, 2 days). The short S•••S contacts are specifically emphasised. (b) Generalised structure of the M_2(TTFTB) MOFs (where, M = Mn^{2+}, Co^{2+}, Zn^{2+} or Cd^{2+}). (Reproduced with permission from reference 120. Copyright 2012 American Chemical Society.)

In these M_2(TTFTB) MOFs (M = Zn^{2+}, Co^{2+}, Mn^{2+} and Cd^{2+}), the non-covalent interactions (*i.e*., π–π stacking) are thought to support efficient orbital overlap between neighbouring TTF moieties that, in turn, provide an extended charge transport pathway within the rigid MOF structure. Partial oxidation of these materials leads to the production of $TTF^{\bullet+}$ sites. This leads to enhanced conductivity ranging from *ca*. 10^{-6} S cm^{-1} for Zn_2(TTFTB) and Co_2(TTFTB) to 10^{-5} S cm^{-1} for Mn_2(TTFTB) and 10^{-4} S cm^{-1} for Cd_2(TTFTB) at 298 K. The through-space charge transport within these MOFs gives rise to charge mobilities that range from 10^{-5} – 10 cm^2 V^{-1} s^{-1}. These values are comparable with those recorded for other common organic semiconductors.

Dincă *et al*. reported another TTF-based MOF (MIT-25),[122] having the empirical formula, $Mg_2H_6(H_3O)(TTFTB)_3$. This particular MOF was prepared *via* the metal assisted self-assembly of what are formally TTFTB molecular triads (*cf*. Fig. 38b). A solid state X-ray structural analysis of MIT-25 revealed the presence of three dimensional hexagonal mesoporous channels, as well as smaller micropores that run parallel to the main channels (Fig. 38a). DFT calculations allowed predictions of the formation energies for the neutral dimer ($[H_4TTFTB]_2$), singly oxidised dimeric ($[H_4TTFTB]_2^{\bullet+}$) and trimeric ($[H_4TTFTB]_3^{\bullet+}$) species, respectively. The resulting values, *viz*. –1.62, –5.52 and –13.73 kcal mol^{-1} for these three forms, respectively, led to the prediction that even the oxidised trimer, $[H_4TTFTB]_3^{\bullet+}$, is readily accessible under conditions of mild oxidation (experimental oxidation potential = +0.34 V vs. Ag/AgCl). This oxidised trimer form is thought to provide electron holes that are fully delocalised across all three TTF moieties (Fig. 38c). Likely as a result of these features, MIT-25 exhibits temperature and humidity-dependent proton conductivity.[123]

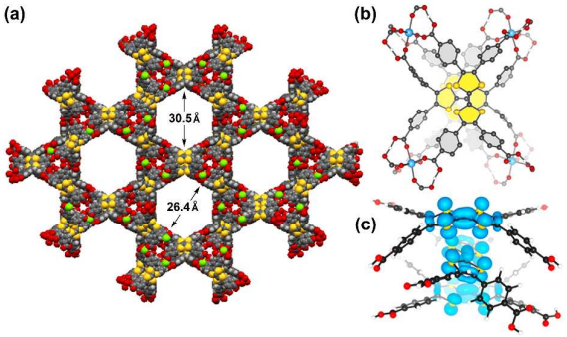

Fig. 38 (a) Space filling model of a portion of the X-ray crystal structure of a Mg(II)-based electroactive MOF (MIT-25) as viewed along the 'c' axis, featuring distinct hexagonal mesopores and micropores. (b) View of the four neighbouring Mg^{2+} coordination environments bridged by a formal TTFTB molecular triad. (c) DFT calculated spin densities of the $(H_4TTFTB)_3^{\bullet+}$ form showing delocalisation across the TTF moiety structure. (Reproduced with permission from reference 122. Copyright 2017 American Chemical Society).

Electrochemical impedance spectroscopic (EIS) measurements of MIT-25 revealed that at 40% relative humidity (RH) the proton conductivity increased from 1.58 × 10^{-5} S cm^{-1} at 298 K to 1.03 × 10^{-4} S cm^{-1} at 358 K, giving an E_a of 0.36 (± 0.0074) eV. At 95% RH, the proton conductivity increased from 6.8 × 10^{-5} S cm^{-1} at 298 K to 5.1 × 10^{-4} S cm^{-1} at 358 K, giving an E_a of 0.40 (± 0.0009) eV.[123] This and related TTF-functionalised MOFs may thus have a role to play as efficient proton conductive materials.

Zuo *et al.* reported two three dimensional Fe(II)-based MOFs[124] constructed using the redox-active *tetrakis*(4-pyridyl) tetrathiafulvalene precursor **53**. These MOFs were found to exhibit

multifunctional magnetic, electronic and optical properties that led to suggestions that they might be suitable for developing electronic devices. It was observed that the Fe(II)-based MOFs derived from **53** exist in the form of (4,6)-linked binodal *sqc11*-type 3D frameworks that undergo a crystal-to-crystal structural transformation upon iodine (I_2) doping (Fig. 39). The I_2-doped MOF not only displays enhanced conductive properties (by 2–3 fold), but also magnetic properties that differ from the undoped form.

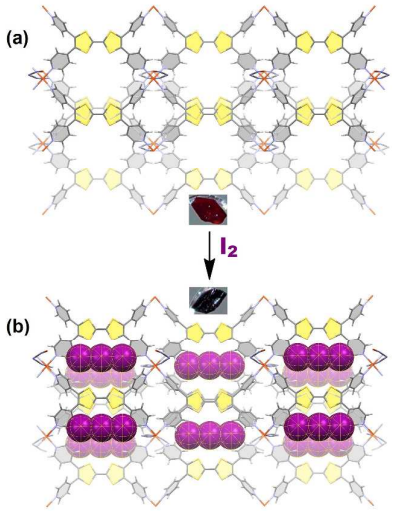

Fig. 39 a) View of the 3D network that makes up the TTF-based Fe(II)-MOF derived from precursor **53** as seen along the 'b' axis and b) view of the 3D network when this system is doped with I_2 as seen along the 'b' axis. Insets: Photographs of the corresponding crystals. This figure was redrawn using data that were originally published in reference 124.

Solid state electrochemical studies revealed that the redox activity of the TTF moiety was maintained in both systems. The initial *sqc11*-type 3D MOF demonstrates incomplete gradual spin-crossover behaviour in accord with a 'light-induced excited spin-state trapping' (LIESST) effect at low temperature. It might therefore see application as a photo- and electronically switchable spin crossover (SCO) material. Other electroactive coordination polymers based on either **H_4TTFTB** or **53** have been reported.[126–128] Although further study is warranted, these systems are expected to display interesting electrochemical, magnetic, catalytic and gas adsorption properties.

10.2. TTF-based COFs. In conjunction with the TTF-based MOFs discussed earlier, TTF building blocks have also been used to synthesise conducting materials based on covalent organic frameworks (COFs). This was done via the controlled self-assembly of 2D-structures at the atomic scale. In contrast to more conventional COFs possessing lower levels of intra-plane π-conjugation,[129,130] the TTF-based COFs display features consistent with higher levels of conjugation within the framework. This makes theses species attractive as potential semi-conducting materials. Open nano-channels are seen within the TTF-based COFs;[131] this allows the incorporation of molecular dopants, such as iodine (I_2) or TCNQ, to enhance CT interactions. Such additions leads to formation of a characteristic mixed valence TTF species with good electrical conductivity. A mechanistic rational for the electrical conductivity seen in the case of TTF-COFs is shown in Fig. 40.

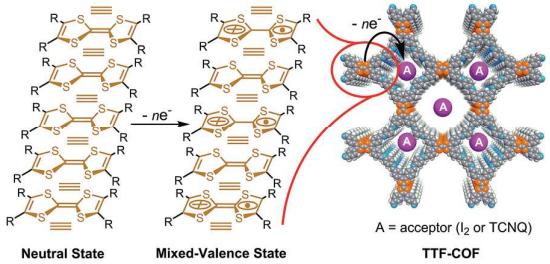

Fig. 40 Mixed-valence state seen in a **TTF-COF** upon doping with an appropriate guest doping. Also shown is the proposed mechanism underlying the observed electrical conductivity. The symbol "≡" indicates the inter-TTF-layer interactions. Reproduced from reference 131 with permission from The Royal Society of Chemistry, copyright 2014.

The first examples of TTF-based COFs were reported concurrently in 2014 by three independent research groups.[131–133] All of them used the same COF building block, *viz*. 2,3,6,7-*tetrakis*(4-formylphenyl)-tetrathiafulvalene (**65**), and a *p*-phenylenediamine linker (**66**) under solvothermal conditions (using mesitylene/dioxane/3 M acetic acid, 120 °C, 72 h) to obtain a 2D porous material, **TTF-Ph-COF** (Scheme 10). This was isolated in the form of either thin films or solid crystalline materials.

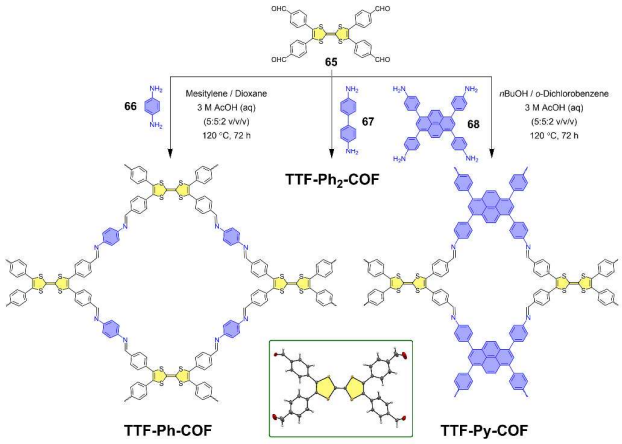

Scheme 10 Synthetic routes to various COFs based on a common precursor, 2,3,6,7-*tetrakis*(4-formylphenyl)-tetrathiafulvalene, **65**, and different linkers (**66–68**). Inset: Single crystal X-ray structures of the precursor **65**. The wavy lines represent the extension of periodic structures.

Zhang, Liu and co-workers[131] reported that the electrical conductivity of a pristine **TTF-Ph-COF** thin film (1.2×10^{-4} S m^{-1}) could be significantly enhanced to 0.28 S m^{-1} upon exposure of the

material to I_2 vapour. The resulting increase in the conductivity was attributed to effective cross-layer radical delocalisation within the mixed-valence TTF stacks present in what can be viewed as being 2D grid-like sheets of the **TTF-Ph-COF**. UV–Vis–NIR and EPR spectral analyses supported the formation of oxidized ($TTF^{\bullet+}$) subunits upon treatment with the I_2 of dopant.

Further investigations by Wang and Zhang *et al.* revealed that the conductivity of **TTF-Ph-COF** could be increased to 1.8×10^{-6} S m^{-1} upon extending the I_2 doping time and upon raising the temperature (Fig. 41).[132]

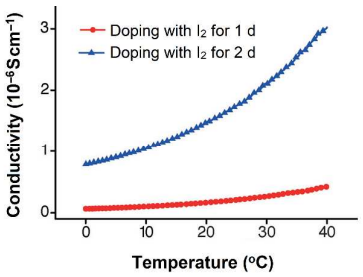

Fig. 41 Enhancement in the electrical conductivity of **TTF-Ph-COF** seen as a function of I_2 doping time and temperature. (This figure is reproduced with permission from reference 132. (Copyright 2014, Wiley-VCH Verlag GmbH & Co. KGaA, Weinheim.)

Jiang *et al*. reported[133] another COF (**TTF-Py-COF**), obtained under solvothermal reaction conditions. This COF was obtained by heating **65** with 1,3,6,8-*tetrakis*(4-aminophenyl)pyrene (**68**) in *n*BuOH/*o*-dichlobenzene/3 M AcOH (Scheme 10). By comparing **TTF-Ph-COF** and **TTF-Py-COF** insights into the role of the linker were obtained. For instance, electrodeless flash-photolysis time-resolved microwave conductivity (FP-TRMC) measurements revealed that **TTF-Ph-COF** has a larger charge-carrier mobility of 0.2 $cm^2V^{-1}s^{-1}$ than **TTF-Py-COF** (0.08 $cm^2V^{-1}s^{-1}$). The conductivities of films containing these two TTF-COFs revealed values of $10^{-5}S^{-1}m^{-1}$ and $10^{-6}S^{-1}m^{-1}$ for **TTF-Ph-COF** and **TTF-Py-COF**, respectively. Th4ese differences were ascribed to differences in packing within the respective layered structures and the associated interlayer separations (*cf*. Fig. 42). These latter valeus were predicted to be 3.71 Å for **TTF-Ph-COF** and 3.87 Å for **TTF-Py-COF** as inferred from density functional tight binding (DFTB) calculations.

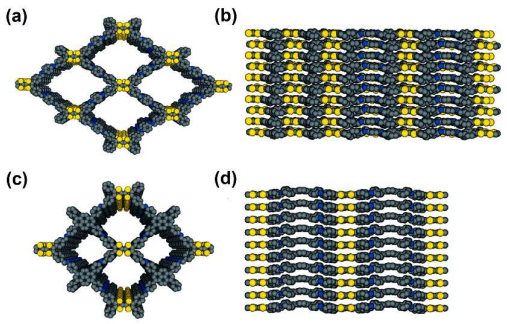

Fig. 42 DFTB predicted slipped stacking structures of **TTF-Ph-COF**, (a) top view and (b) side view and **TTF-Py-COF** (c) top view and (d) side view respectively. (Reproduced with permission from reference 133. Copyright 2014, Wiley-VCH Verlag GmbH & Co. KGaA, Weinheim.)

Wang and Wan *et al*.[134,135] providerd experimental support for these latter predicted values by carrying out on-surface high-resolution scanning tunnelling microscopic (STM) analyses of **TTF-Py-COF** and its higher analogue, **TTF-Ph_2-COF**, obtained from **65** and 1,1'-biphenyl-4,4'-diamine, **67** (Scheme 10). The results provided direct support for the proposed eclipsed stacking between the TTF-COFs.

11. TTF-catenanes and "molecular machines"

Catenanes (from the Greek "*catena*" meaning chain) are classic molecular systems containing two or more interlocked rings, which cannot be separated without the breaking of at least one covalent bond. Numerous examples of catenanes have been reported in recent years and the majority of those have been constructed by taking advantage of supramolecular interactions to promote their synthesis. A number of elegant catenanes incorporate one or more electroactive TTF units within their structures; some classic examples, *e.g.*, **69–79**[136–142], are shown in Chart 12.

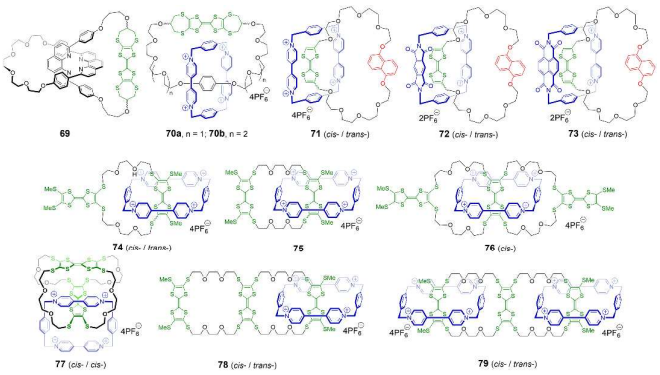

Chart 12 Chemical structures of representative TTF-based catenanes.

Many TTF-containing catenanes have been prepared with a view towards creating molecular switches and machines. The three possible redox states of the TTF unit, as well as the typically reversible interconversion between these states, makes TTF-containing catenanes and related mechanically interlocked molecules (MIMs) attractive for controlling molecular movement and thus for the creation of devices that function at the molecular level. In this section, we provide a brief summary of TTF-based macrocycles that have been studied as potential molecular switches and machines.

A number of [2]catenanes that incorporate both polyether-bridged tetramercapto-TTF donor subunits and cyclic

cyclobis(paraquat-*p*-phenylene) electron acceptor moieties have been reported. Representative syntheses are shown in Scheme 11. For example, treatment of the [2]pseudorotaxane **81** with the diiodo glycol precursor **80** under high dilution condition in the presence of a catalytic amount of base gives the Cu(I)-complex of the catenane **69** as its hexafluorophosphate salt *(i.e.*, **69**•Cu•PF_6). Subsequent demetallation, involving treatment with KI, gave the free form of the catenane (**69**; Scheme 11a).

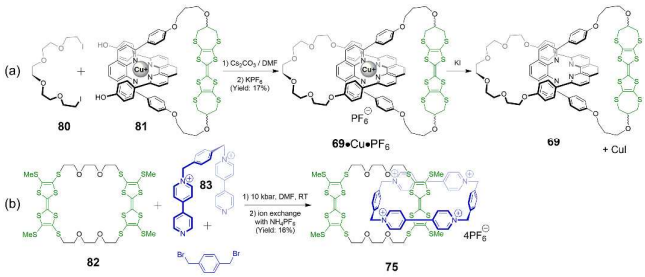

Scheme 11 Two synthetic routes used to construct TTF-based [2]catenanes.

The TTF group has also been used as a template to self-assemble catenanes containing one or more cyclobis(paraquat-*p*-phenylene) rings. For instance, mixing macrocycle **82**, which incorporates two TTF units, the horseshoe shaped dication **83** and 1,4-bis(bromomethyl)benzene under high-pressure conditions (10 kbar) results in the formation of the corresponding [2]catenanes **75** (Scheme 11b).

In 1998 Balzani, Stoddart, Venturi and Williams *et al*. reported[139] the [2]catenane, **71** (Chart 12). This system incorporates a TTF unit and a 1,5-dioxynaphthalene (DNP) moiety within one ring and a cyclobis(paraquat-*p*-phenylene) acceptor as the other ring. It was shown that **71** behaves as a redox-driven molecular machine (Scheme 12) with the reversible redox features of the TTF unit being used to control the requisite motion at the molecular level. Specifically, it was demonstrated that, upon oxidation of the TTF unit (by either chemical or electrochemical means), the cyclobis(paraquat-*p*-phenylene) ring was forced to move from a point close to the oxidised and positively charged TTF subunit to near the DNP donor moiety. This conversion afforded the maroon coloured isomer **71b**. Subsequent reduction was found to regenerate the original dark green isomer **71a**. The motion could also be monitored by ^{1}H NMR spectroscopy, UV–Vis spectroscopy or cyclic voltammetry (CV).

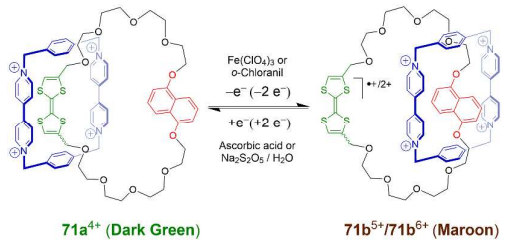

Scheme 12 Chemically and electrochemically triggered redox-switching of the TTF-based [2]catenane **71**.

Cooke and Stoddart, *et al*. reported[142] two donor–acceptor based mechanically interlocked 'molecular flasks', **84** and **85** (Chart 13). These systems are [3]catenanes, comprised of two identical macrocycles having either a TTF unit and a DNP moiety (**86**) or a TTF and a butadiyne group (**88**) incorporated in the same ring.

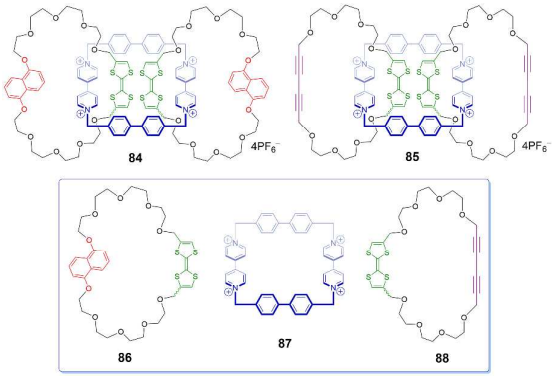

Chart 13 Chemical structures of TTF-based [3]catenanes **84** and **85** and the individual components from which they are formally comprised (**86**–**88**).

In both [3]catenanes, the two redox-active TTF subunits are positioned within the same tetracationic ring (formally **87**). Upon oxidation these catenanes support the formation of stable mechanically linked internal pseudo dimers of TTF (*i.e*., formal $(TTF)_2^{\bullet+}$ and $(TTF^{\bullet+})_2$ states respectively; *cf*. Figs. 43b,c) under ambient conditions.

The high stability of the electrochemically accessible dimeric states seen for **84** and **85** (Fig. 43) is ascribed to the underlying MIM structures. The associated interlocking provides both an ideal three dimensional geometric arrangement and enforces what are effectively ultrahigh local concentrations of the individual TTF species. These dimerisation events represent an affinity umpolung in that the stabilisation provided by mixed-valence $(TTF)_2^{\bullet+}$ and radical-cation $(TTF^{\bullet+})_2$ states inside the "molecular flasks" serve to replace more traditional TTF–bipyridinium interactions.

By replacing the DNP station with a butadiyne group it was found that the distribution of states could be made to favour further formation of the TTF radical-cation dimer state, $(TTF^{\bullet+})_2$, (*i.e*., from 60% to 100%). Support for this conclusion came from a number of solution phase studies, including cyclic voltammetry, spectroelectrochemistry, UV–Vis–NIR and EPR spectroscopies, as well as solid state X-ray diffraction analyses (*cf*., Figs. 44a,b). Accompanying DFT calculations provided support for the notion that first paramagnetic mixed-valence dimers are stabilised and that diamagnetic radical-cation dimers are obtained upon oxidation of the [3]catenanes **84** and **85**.

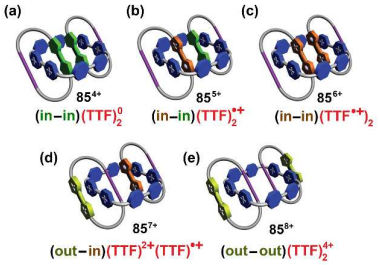

Fig. 43 Cartoon representations of all the possible conformations of [3]catenanes, **85**. (a) Neutral TTF–bipyridinium CT dimer, $(TTF)_2$; (b) mixed-valence dimer, $(TTF)_2^{\bullet+}$; (c) radical-cation dimer, $(TTF^{\bullet+})_2$; (d) dication–radical-cation species, $(TTF)^{2+}(TTF)^{\bullet+}$; and (e) tetracationic species, $(TTF)_2^{4+}$ respectively. This Fig. was redrawn using the data that were originally published in reference 142.

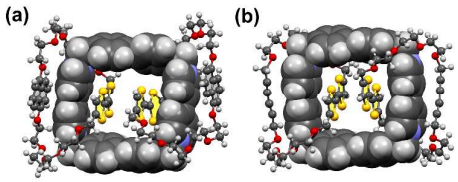

Fig. 44 Single crystal X-ray structures (a) and (b) of **84** and **85**, respectively. Residual solvent molecules and anions are omitted for clarity. This Figure was redrawn using the data that were originally published in reference 142.

Continuous wave EPR (CW EPR) spectral studies of **84** and **85** under ambient conditions provided support for the stepwise chemical oxidation of these [3]catenanes.[143] This oxidation triggers a number of chemical events, including the formation of formal isomers as shown in Fig. 45.

In these studies, oxidation was effected *via* the gradual addition of $Fe(ClO_4)_3$. Formation of mixed-valence states of $\mathbf{84}^{5+}$ and $\mathbf{85}^{5+}$ were observed upon addition of 1.0 equiv. of this chemical oxidant (Figs. 45a,d). Addition of 2.0 equiv. of the oxidant produced notable changes in the EPR spectra of $\mathbf{84}^{6+}$ (Fig. 45b) and $\mathbf{85}^{6+}$ (Fig. 45e). In the case of $\mathbf{85}^{6+}$, attenuation of the radical signal was seen, an effect ascribed to the strong spin-coupling between the two neighbouring $TTF^{\bullet+}$ units. However, in the case of $\mathbf{84}^{6+}$, only a minor decrease in the EPR signal intensity was observed (*cf*. Fig. 45b). This disparity was rationalised in terms of the presence of the EPR-active species $\mathbf{84}_{out}^{6+}$ where the individual $TTF^{\bullet+}$ units (corresponding to **86**) are exposed outside the macrocyclic system formally made up of **87**. CV and UV–Vis spectral studies provided support for the conclusion that once the corresponding $\mathbf{84}_{in}^{6+}$ species is generated in the medium (wherein individual $TTF^{\bullet+}$ units of **86** are brought into close proximity within the macrocyclic system **87**), an equilibrium arises between $\mathbf{84}_{in}^{6+}$ and $\mathbf{84}_{out}^{6+}$. EPR analyses led to the suggestion that the equilibrium distribution is approximately 60:40 in favour of the $\mathbf{84}_{in}^{6+}$ state. Further oxidation of both [3]catenanes, (*i.e.*, $\mathbf{84}_{in/out}^{6+}$ and $\mathbf{85}^{6+}$) with 4.0 equiv. of the oxidant results in the formation of the corresponding fully oxidised EPR-silent states $\mathbf{84}^{8+}$ (the gradual quenching of EPR signal is shown in Fig. 45c) and $\mathbf{85}^{8+}$ (Fig. 45g), respectively.

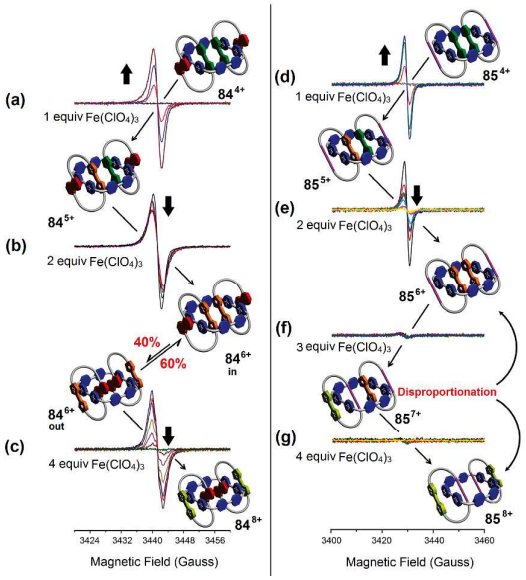

Fig. 45 CW EPR spectra of **84** (left side) and **85** (right side) as 0.3 mM solutions in MeCN recorded at 295 K recorded upon stepwise chemical oxidation with $Fe(ClO_4)_3$. (Reproduced with permission from reference 143. Copyright 2011 American Chemical Society.)

Examples of TTF-bearing metallo[*n*]catenanes (where *n* = 2 or 3, respectively) have been reported recently.[144,145] Here, the basic design strategy has involved the use of metal–ligand coordination with donor–acceptor supramolecular interactions to drive catenane formation. Generally, Pd^{2+} or Pt^{2+} cations have been employed in this regard so as to take advantage of the square planar coordination geometries preferred by these cations. Examples of the precursors and resulting metallo[*n*]catenanes are provided in Chart 14.

Liu *et al*. reported a dynamic redox switch, **92**, consisting of a donor–acceptor metallo[2]catenane formed by the self-assembly of a diimide-based metallomacrocycle, **89**•$4NO_3^-$ and a crown ether precursor **86**. Switching in the form of self-assembly and disassembly was demonstrated under conditions of electrochemical control with the redox effects being ascribed to the presence of the TTF moiety.[144]

Stoddart *et al*. reported[145] mechanically interlocked TTF-containing frameworks consisting of [3]catenanes and Solomon link isomers derived from precursors **86**, **90**•$8PF_6^-$ and **91** (Charts 13 and 14). These systems were explored in an effort to determine the effect of topology on the redox states of closely interacting TTF subunits. It was found that the three dimensional alignment of two electroactive TTF units triggers the assembly of an organoplatinum molecular square and directs the formation of two mechanical conformers (Fig. 46).

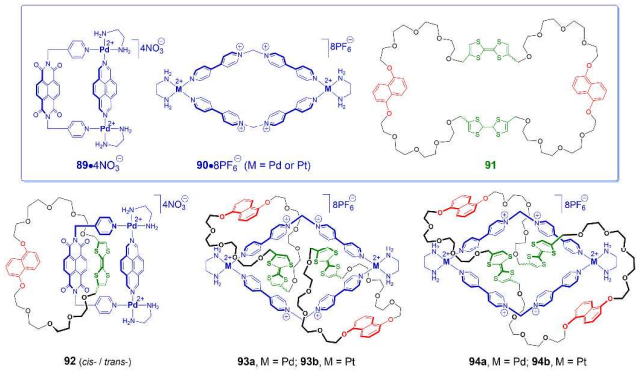

Chart 14 Chemical structures of representative precursors used to construct TTF-based metalla[*n*]catenanes and examples of metalla[*n*]catenane based redox-switches.

The topological constraints present in the molecular Solomon link introduce a high level of dynamic structural complexity over the geometric changes that occur as the result of electronic modulation of the TTF units within these catenanes. Detailed electrochemical analyses revealed a fundamental relationship between topology and the redox properties of these radically configurable isomers (*i.e.*, **72**$^{8+}$, **73**$^{8+}$ and **71**⊂**70**$^{8+}$).

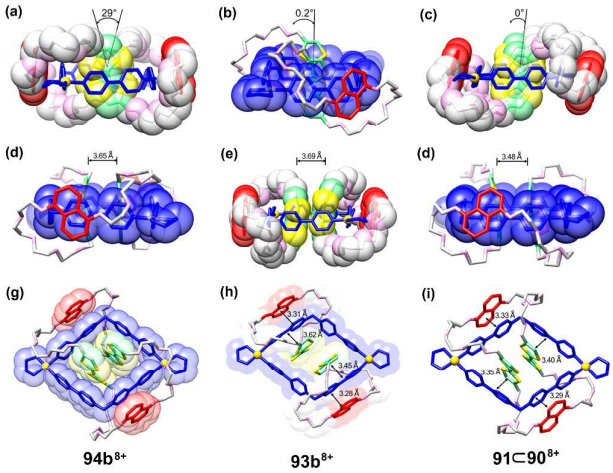

Fig. 46 Single crystal X-ray structures of the molecular Solomon link **94b**$^{8+}$ (a, d and g); [3]catenanes **93b**$^{8+}$ (b, e and h), and the ring-in-ring complex **91**⊂**90**$^{8+}$ (c, f and i), respectively. (Reproduced with permission from reference 145. Copyright 2014 American Chemical Society.)

12. Biological aspects of TTF-fused systems

In living systems, including plants and animals, the active transport of ions and molecules is necessary to create the concentration gradients that underlie nearly all biological activities. A recognised challenge for supramolecular chemists has been to replicate this active transport using various artificial molecular motifs. In this context, TTF functionalised mechanically interlocked molecular systems (MIMs),[146] artificial molecular machines (AMMs),[147] and other systems constructed by means of either TTF or exTTF are attractive. This is because, at least in principle, ion recognition and release could be induced by means of electrochemical switching of the constituent TTF or exTTF moiety. TTF-switching is also of interest in the context of controlling the properties of systems designed to mimic other important functions, such as charge capture and conformational motion. Several promising TTF-based systems with potential biological ramifications have been described recently. None is macrocyclic in nature. Therefore, the work in question nominally falls outside the scope of this review. However, since it sets the stage for future progress, a brief summary is appropriate here.

Bio-inspired nanotubular cyclopeptidic heterodimers bearing electroactive exTTF moiety were reported in 2007 by Brea, *et al.*[148] and put forward as light-harvesting/light-converting hybrid ensembles. Such systems could function as possible switchable ion transporters. The same is true for TTF-labelled oligodeoxynucleotides, examples of which were reported by Fermín and co-workers.[149]

In a separate line of investigation, Bancafort and Ribas demonstrated that a self-assembled cofacial Zn(II)-porphyrin nanocage could behave as a robust singlet oxygen ($^1O_2$) photosensitiser with tunable features.[150] In this study, the production of $^1O_2$ was inferred through oxygenation of the exTTF-based coordinating ligand **56** (*cf*. Chart 10).

Martín and co-workers reported[151] a variety of electroactive peptide-based exTTF derivatives that support the formation of different aggregated states depending on the environmental conditions. It was found that formation of either a metastable state or a thermodynamically favoured supramolecular polymer could occur, with the product obtained depending on the concentration and ionic strength of the medium. Electrochemical changes involving the exTTF moiety provided another element of control. Ultimately, these and other redox switchable systems could see use as drug delivery agents or biomimetics of key regulatory functions. This is an area that is still in its infancy. Much work remains to be done. However, it is likely that the redox switching capability provided by one or more TTF moieties incorporated into responsive systems will help bridge the gap between fundamental chemistry and biology in ways that might not yet be envisioned.

13. Conclusion and future prospects

This review article highlights recent work involving TTF-fused macrocyclic systems. The host–guest interactions between TTF-based calixpyrroles, macrocyclic tapes, cyclophanes, cryptands, cavitands and metalla-cages with various guest molecules are discussed. The electron donating ability of the TTF subunit has been exploited in a number of supramolecular host–guest systems and has given rise to the preparation of sensors, molecular switches and catalysts for specific reactions. The charge transfer character seen in the case of many TTF-macrocycle complexes allows for the detection of numerous analytes, while the redox active nature of the TTF subunit has provided the predicate for the construction of new state-of-art systems capable of capturing and storing charge or

binding and releasing specific neutral guest through controlled electrochemical switching. TTF-based mesoporous hybrid metal-organic frameworks are now known, as are electroactive TTF-containing systems that show promise for the construction of electronic and spintronic devices. Developments in both synthetic TTF chemistry and supramolecular chemistry have made it possible to construct many elaborate systems, with applications in the chemical, physical and biological world. Much of the synthetic effort associated with TTF-containing systems has been focused on TTF-tetrathiolates on account of their facile preparation and strong nucleophilicity. Recent access to pyrrolo-annelated TTFs possessing strong π-donor properties offers additional opportunities for the design and construction of redox active supramolecular systems. To quote, Julius Rebek,[152] "The question is no longer *if* something can be built, but *what* to build and *why*". In this context, TTF-based superstructures appear particularly promising. Nevertheless, a deeper understanding is still needed such that the control parameters governing TTF-containing macrocyclic hosts can be fully exploited. It is hoped that this review will provide an initial foundation for this future understanding.

List of abbreviations

3D	three dimensional
A	π-electron acceptor
AMBER	assisted model building with energy refinement
AMMs	artificial molecular machines
BIQ	bisimidazolium quinine (1,3,5,7-tetramesityl-4,8-dioxo-3,4,7,8-tetrahydrobenzo[1,2-d:4,5-d']-diimidazole-1,5-diium)
BPTTF	bis(pyrrolo)tetrathiafulvalene
C[4]P	calix[4]pyrrole
C_{60}	buckminsterfullerene
cod	cyclooctadiene
CS	charge separated
CT	charge transfer
CTV	cyclotriveratrylene
CV	cyclic voltammogram
CW EPR	continuous wave electron paramagnetic resonance
D	π-electron donor
dctfb	dichlorotrifluorobenzene
DFT	density functional theory
DFTB	density functional tight binding
DNA	deoxyribonucleic acid
DNP	1,5-dioxynaphthalene
DMSO	dimethyl sulfoxide
DOSY-NMR	diffusion ordered nuclear magnetic resonance
DPV	differential pulse voltammetry
dppp	1,3-*bis*(diphenylphosphino)propane
dppf	1,1'-*bis*(diphenylphosphino)ferrocene
EIS	electrochemical impedance spectroscopy
en	ethylenediamine
EPR	electron paramagnetic resonance
ET	electron transfer
exTTF	extended-tetrathiafulvalene
exTTFAQ	9,10-bis(1,3-dithiol-2-ylidene)-9,10-dihydroanthracene-based extended-tetrathiafulvalene
F_4TCNQ	2,3,5,6-tetrafluoro-7,7,8,8-tetracyanoquinodimethane
FTIR	fourier transform infrared spectroscopy
FT-TRMC	flash-photolysis time-resolved microwave conductivity
HRMS	high resolution mass spectrometry
MeCN	acetonitrile
MIMs	mechanically interlocked molecules
MM+	molecular mechanics
MPTTF	monopyrrolotetrathiafulvalene
NDA	1,4,5,8-naphthalenetetracarboxylic dianhydride
NIR	near-infrared
NMR	nuclear magnetic resonance
OTf	trifluoromethane-sulfonate
PET	photoinduced electron transfer
PhCl	chlorobenzene
PhCN	benzonitrile
ppb	parts per billion
RH	relative humidity
sExTTF	super-π-extended tetrathiafulvalene
STM	scanning tunnelling microscopy
TBACl	tetrabutylammonium chloride
TCE	tetrachloroethane
TCNQ	tetracyaniquinodimethane
TEA	triethylamine
TEACl	tetrakis-ethylammonium chloride
TEG	triethylene glycol monomethyl ether
TNB	1,3,5-trinitrobenzene
TNF	2,4,7-trinitro-9-fluorenylidenemalononitrile
TNP	2,4,6-trinitrophenol (picric acid)
TNT	2,4,6-trinitrotoluene
TOA^+	tetraoctylammonium cation
TTF	tetrathiafulvalene
TTFV	tetrathiafulvalene vinylogue

Conflicts of interest

The authors declare no competing financial interest.

Acknowledgements

AJ is thankful to JLS for his continuous support and encouragement for doing chemistry, and to Shanghai University for providing research facility. SB greatly acknowledges The Danish Council for Independent Research, Technology, and Production Sciences (FTP, Project 5054-00052). MI thanks JSPS Grant-in-Aid for scientific research (Nos. JP16K05700 and JP17H05377). MS thanks the CNRS, Univ. Angers and ANR (JCJC program, ANR-14-CE08-0001 BOMBER, S.G). JOJ thanks the Villum Foundation and the Danish Natural Science Research Council (FNU, Project 11-106744) for financial support. JLS acknowledges the US National Science Foundation (grant CHE-1402004), the Robert A. Welch Foundation and N.13-G210-18-209 from Shanghai University for support of this work.

Notes and references

1 F. Wudl, G. M. Smith and E. J. Hufnagel, *J. Chem. Soc. D* 1970, **21**, 1453–1454.
2 F. Wudl, D. Wobschall and E. J. Hufnagel, *J. Am. Chem. Soc.*, 1972, **94**, 670–672.
3 J. Ferraris, D. O. Cowan, V. Walatka and J. H. Perlstein, *J. Am. Chem. Soc.*, 1973, **95**, 948–949.
4 M. R. Bryce, *Chem. Soc. Rev.*, 1991, **20**, 355–390.
5 M. R. Bryce, *J. Mater. Chem.*, 1995, **5**, 1481–1496.
6 M. R. Bryce, *Adv. Mater.*, 1999, **11**, 11–23.
7 M. R. Bryce, *J. Mater. Chem.*, 2000, **10**, 589–598.
8 M. B. Nielsen, C. Lomholt and J. Becher, *Chem. Soc. Rev.*, 2000, **29**, 153–164.
9 J. L. Segura and N. Martín, *Angew. Chem., Int. Ed.*, 2001, **40**, 1372–1409.
10 J. O. Jeppesen and J. Becher, *Eur. J. Org. Chem.*, 2003, **17**, 3245–3266.
11 J. Yamada, H. Akutsu, H. Nishikawa and K. Kikuchi, *Chem. Rev.*, 2004, **104**, 5057–5083.
12 P. Frère and P. J. Sakabara, *Chem. Soc. Rev.*, 2005, **34**, 69–98.
13 D. Canevet, M. Sallé, G. X. Zhang, D. Q. Zhang and D. B. Zhu, *Chem. Commun.*, 2009, 2245–2269.
14 M. Shatruk and L. Ray, *Dalton Trans.*, 2010, **39**, 11105–11121.
15 F. G. Brunetti, J. L. López, C. Atienza and N. Martín, *J. Mater. Chem.*, 2012, 4188–4205.
16 J. J. Bergkamp, S. Decurtins and S.-X. Liu, *Chem. Soc. Rev.*, 2015, **44**, 863–874.
17 M. Iyoda and M. Hasegawa, *Beilstein J. Org. Chem.*, 2015, **11**, 1596–1613.
18 F. Pop and N. Avarvari, *Chem. Commun.*, 2016, **52**, 7906–7927.
19 V. A. Azov, *Tetrahedron Lett*., 2016, **57**, 5416–5425.
20 A. Jana, M. Ishida, J. S. Park, S. Bähring, J. O. Jeppesen and J. L. Sessler, *Chem. Rev*., 2017, **117**, 2641–2710.
21 J. M. Fabre, *Chem. Rev.*, 2004, **104**, 5133–5150.
22 A. Kobayashi, E. Fujiwara and H. Kobayashi, *Chem. Rev.*, 2004, **104**, 5243–5264.
23 D. Lorcy, N. Bellec, M. Fourmigue and N. Avarvari, *Coord. Chem. Rev.*, 2009, **253**, 1398–1438.
24 S. Rabaça and M. Almeida, *Coord. Chem. Rev.*, 2010, **254**, 1493–1508.
25 J. O. Jeppesen, M. B. Nielsen and J. Becher, *Chem. Rev.*, 2004, **104**, 5115–5131.
26 C. Rovira, *Chem. Rev.*, 2004, **104**, 5289–5317.
27 J. G. Hansen, K. S. Bang, N. Thorup and J. Becher, *Eur. J. Org. Chem.*, 2000, 2135–2144.
28 K. B. Simonsen, K. W. Zong, R. D. Rogers, M. P. Cava and J. Becher, *J. Org. Chem.*, 1997, **62**, 679–686.
29 J. S. Park, C. Bejger, K. R. Larson, K. Nielsen, A. Jana, V. M. Lynch, J. O. Jeppesen, D. Kim and J. L. Sessler, *Chem. Sci.*, 2012, **3**, 2685–2689.
30 K. A. Nielsen, J. O. Jeppesen and E. Levillain, *Angew. Chem., Int. Ed*., 2003, **42**, 187–191.
31 K. A. Nielsen, W.-S. Cho, J. Lyskawa, E. Levillain, V. M. Lynch, J. L. Sessler and J. O. Jeppesen, *J. Am. Chem. Soc.*, 2006, **128**, 2444–2451.
32 K. A. Nielsen, W.-S. Cho, J. O. Jeppesen, V. M. Lynch, J. Becher and J. L. Sessler, *J. Am. Chem. Soc.*, 2004, **126**, 16296–16297.
33 T. Duedal, K. A. Nielsen, G. Olsen, C. B. G. Rasmussen, J. Kongsted, E. Levillain, T. Breton, E. Miyazaki, K. Takimiya, S. Bähring and J. O. Jeppesen, *J. Org. Chem*., 2017, **82**, 2123–2128.
34 J. S. Park, F. Le Derf, C. M. Bejger, V. M. Lynch, J. L. Sessler, K. A. Nielsen, C. Johnsen and J. O. Jeppesen, *Chem.– Eur. J.*, 2010, **16**, 848–854, and the references therein.
35 W. Zhu, J. S. Park, J. L. Sessler and A. Gaitas, *Appl. Phys. Lett.*, 2011, **98**, 123501.
36 F. G. Bosco, M. Bache, E.-T. Hwu, C. H. Chen, S. S. Andersen, K. A. Nielsen, S. S. Keller, J. O. Jeppesen, I.-S. Hwang and A. Boisen, *Sens. Actuators B* 2012, **171–172**, 1054–1059.
37 E. H. Witlicki, S. Bähring, C. Johnsen, M. V. Solano, K. A. Nielsen, D. W. Silverstein, C. W. Marlatt, L. Jensen, J. O. Jeppesen and A. H. Flood, *Chem. Commun*., 2017, **53**, 10918–10921.
38 K. A. Nielsen, W.-S. Cho, G. H. Sarova, B. M. Petersen, A. D. Bond, J. Becher, F. Jensen, D. M. Guldi, J. L. Sessler and J. O. Jeppesen, *Angew. Chem., Int. Ed.*, 2006, **45**, 6848–6853.
39 C. M. Davis, J. M. Lim, K. R. Larsen, D. S. Kim, Y. M. Sung, D. M. Lyons, V. M. Lynch, K. A. Nielsen, J. O. Jeppesen, D. Kim, J. S. Park and J. L. Sessler, *J. Am. Chem. Soc.*, 2014, **136**, 10410–10417.
40 K. A. Nielsen, G. H. Sarova, L. Martín-Gomis, F. Fernández-Lázaro, P. C. Stein, L. Sanguinet, E. Levillain, J. L. Sessler, D. M. Guldi, Á. Sastre-Santos and J. O. Jeppesen, *J. Am. Chem. Soc*., 2008, **130**, 460–462.
41 K. A. Nielsen, L. Martín-Gomis, G. H. Sarova, L. Sanguinet, D. E. Gross, F. Fernández-Lázaro, P. C. Stein, E. Levillain, J. L. Sessler, D. M. Guldi, Á. Sastre-Santos and J. O. Jeppesen, *Tetrahedron* 2008, **64**, 8449–8463.
42 J. S. Park, E. Karnas, K. Ohkubo, P. Chen, K. M. Kadish, S. Fukuzumi, C. W. Bielawski, T. W. Hudnall, V. M. Lynch and J. L. Sessler, *Science* 2010, **329**, 1324–1327.
43 S. Fukuzumi, K. Ohkubo, Y. Kawashima, D. S. Kim, J. S. Park, A. Jana, V. M. Lynch, D. Kim and J. L. Sessler, *J. Am. Chem. Soc.*, 2011, **133**, 15938–15941.
44 C. M. Davis, Y. Kawashima, K. Ohkubo, J. M. Lim, D. Kim, S. Fukuzumi and J. L. Sessler, *J. Phys. Chem. C*, 2014, **118**, 13503–13513.
45 C. M. Davis, K. Ohkubo, A. D. Lammer, D. S. Kim, Y. Kawashima, J. L. Sessler and S. Fukuzumi, *Chem. Commun.*, 2015, **51**, 9789–9792.
46 D.-S. Kim, V. M. Lynch, K. A. Nielsen, C. Johnsen, J. O. Jeppesen and J. L. Sessler, *Anal. Bioanal. Chem*., 2009, **395**, 393–400.
47 T. Poulsen, K. A. Nielsen, A. D. Bond and J. O. Jeppesen, *Org. Lett*., 2007, **9**, 5485–5488.
48 M. Bendikov, F. Wudl and D. F. Perepichka, *Chem. Rev*., 2004, **104**, 4891–4945.
49 D. Canevet, E. M. Pérez and N. Martín, *Angew. Chem., Int. Ed*., 2011, **50**, 9248–9259.
50 M. R. Bryce, A. S. Bastanov, T. Fin, T. K. Hansen, J. A. K. Howard, M. Kamenjicki, I. K. Lednev and S. A. Asher, *Chem. Commun.*, 2000, 295–296.
51 M. R. Bryce, A. S. Batsanov, T. Finn, T. K. Hansen, A. J. Moore, J. A. K. Howard, M. Kamenjicki, I. K. Lednev and S. A. Asher, *Eur. J. Org. Chem.*, 2001, 933–940.
52 A. Ohta, T. Numae, Y. Yamashita, K. Fujimori, *Heterocycles*, 2006, **67**, 665–678.
53 C. A. Christensen, A. S. Batsanov, M. R. Bryce and J. A. K. Howard, *J. Org. Chem*., 2001, **66**, 3313–3320.

54 M. Shao, P. Dongare, L. N. Dawe, D. W. Thompson and Y. Zhao, *Org. Lett*., 2010, **12**, 3050–3053.
55 M. C. Díaz, B. M. Illescas, N. Martín, J. F. Stoddart, M. A. Canales, J. Jiménez-Barbero, G. Sarova and D. M. Guldi, *Tetrahedron* 2006, **62**, 1998–2002.
56 J. Santos, B. Grimm, B. M. Illescas, D. M. Guldi and N. Martín, *Chem. Commun.*, 2008, 5993–5995.
57 B. Grimm, J. Santos, B. M. Illescas, A. Muñoz, D. M. Guldi and N. Martín, *J. Am. Chem. Soc*., 2010, **132**, 17387–17389.
58 L. Moreira, J. Calbo, R. M. Krick Calderon, J. Santos, B. M. Illescas, J. Aragó, J.-F. Nierengarten, D. M. Guldi, E. Ortí and N. Martín, *Chem. Sci*., 2015, **6**, 4426–4432.
59 L. Moreira, B. M. Illescas and N. Martín, *J. Org. Chem.*, 2017, **82**, 3347–3358.
60 E. M. Pérez, L. Sánchez, G. Fernández and N. Martín, *J. Am. Chem. Soc.*, 2006, **128**, 7172–7173.
61 D. Canevet, E. M. Pérez and N. Martín in "Organic Nanomaterials", Eds: T. Torres and G. Bottari, Wiley VCH, 2013.
62 H. Isla, M. Gallego, E. M. Pérez, R. Viruela, E. Ortí and N. Martín, *J. Am. Chem. Soc*., 2010, **132**, 1772–1773.
63 D. Canevet, M. Gallego, H. Isla, A. de Juan, E. M. Pérez and N. Martín, *J. Am. Chem. Soc.*, 2011, **133**, 3184–3190.
64 H. Isla, E. M. Pérez and N. Martín, *Angew. Chem., Int. Ed.*, 2014, **53**, 5629–5633.
65 A. de Juan, Y. Pouillon, L. Ruiz-González, A. Torres-Pardo, S. Casado, N. Martín, Á. Rubio and E. M. Pérez, *Angew. Chem., Int. Ed*., 2014, **53**, 5394–5400.
66 A. de Juan, M. M. Bernal and E. M. Pérez, *ChemPlusChem*, 2015, **80**, 1153–1157.
67 J.-B. Giguère and J.-F. Morin, *J. Org. Chem*., 2015, **80**, 6767–6775.
68 J. W. Steed, P. C. Junk, J. L. Atwood, M. J. Barnes, C. L. Raston and R. S. Burkhalter, *J. Am. Chem. Soc.*, 1994, **116**, 10346–10347.
69 E. Huerta, H. Isla, E. M. Pérez, C. Bo, N. Martín and J. de Mendoza, *J. Am. Chem. Soc*., 2010, **132**, 5351–5353.
70 K. Mulla, H. Shaik, D. W. Thompson and Y. Zhao, *Org. Lett*., 2013, **15**, 4532–4535.
71 S. Mendoza, L. A. Godínez and A. E. Kaifer, *Supramol. Chem*., 2004, **16**, 165–169.
72 M. Frei, F. Diederich, R. Tremont, T. Rodriguez and L. Echegoyen, *Helv. Chim. Acta*, 2006, **89**, 2040–2057.
73 A. Ikeda and S. Shinkai, *Chem. Rev*., 1997, **97**, 1713–1734.
74 J. S. Kim and D. T. Quang, *Chem. Rev*., 2007, **107**, 3780–3799.
75 R. Joseph and C. P. Rao, *Chem. Rev*., 2011, **111**, 4658–4702.
76 S. K. Kim, V. M. Lynch, N. J. Young, B. P. Hay, C.-H. Lee, J. S. Kim, B. A. Moyer and J. L. Sessler, *J. Am. Chem. Soc*., 2012, **134**, 20837–20843.
77 S. K. Kim, G. I. Vargas-Zúñiga, B. P. Hay, N. J. Young, L. H. Delmau, C. Masselin, C.-H. Lee, J. S. Kim, V. M. Lynch, B. A. Boyer and J. L. Sessler, *J. Am. Chem. Soc*., 2012, **134**, 1782–1792.
78 S. K. Kim and J. L. Sessler, *Acc. Chem. Res*., 2014, **47**, 2525–2536.
79 M. H. Düker, R. Gómez, C. M. L. Vande Velde and V. A. Azov, *Tetrahedron Lett*., 2011, **52**, 2881–2884.
80 M. H. Düker, H. Schäfer, M. Zeller and V. A. Azov, *J. Org. Chem*., 2013, **78**, 4905–4912.
81 M. H. Düker, F. Kutter, T. Dülcks and V. A. Azov, *Supramol. Chem*., 2014, **26**, 552–560.
82 K. R. Korsching, H. Schäfer, J. Schönborn, A. Nimthong-Roldán, M. Zeller and V. A. Azov, *RSC Adv*., 2015, **5**, 82633–82637.
83 M. H. Lee, Q.-Y. Cao, S. K. Kim, J. L. Sessler and J. S. Kim, *J. Org. Chem*., 2011, **76**, 870–874.
84 B.-T. Zhao, M.-J. Blesa, N. Mercier, F. Le Derf and M. Sallé, *New J. Chem*., 2005, **29**, 1164–1167.
85 B.-T. Zhao, M.-J. Blesa, N. Mercier, F. Le Derf and M. Sallé, *J. Org. Chem*., 2005, **70**, 6254–6257.
86 B.-T. Zhao, M.-J. Blesa, N. Mercier, F. Le Derf and M. Sallé, *Supramol. Chem*., 2005, **17**, 465–468.
87 J. Lyskawa, M. Sallé, J.-Y. Balandier, F. Le Derf, E. Levillain, M. Allain, P. Viel and S. Palacin, *Chem. Commun.,* 2006, 2233–2235.
88 M.-J. Blesa, B.-T. Zhao, M. Allain, F. Le Derf and M. Sallé, *Chem. – Eur. J*., 2006, **12**, 1906–1914.
89 B.-T. Zhao, M.-J. Blesa, F. Le Derf, D. Canevet, C. Benhaoua, M. Mazari, M. Allain and M. Sallé, *Tetrahedron* 2007, **63**, 10768–10777.
90 B.-T. Zhao, Z. Zhou, Z.-N. Yan, E. Belhadj, F. Le Derf and M. Sallé, *Tetrahedron Lett*., 2010, **51**, 5815–5818.
91 B.-T. Zhao, Q.-M. Peng, X.-M. Zhu, Z.-N. Yan and W.-M. Zhu, *J. Org. Chem*., 2015, **80**, 1052–1058.
92 P. Blanchard, N. Svenstrup, J. Rault-Berthelot, A. Riou and J. Becher, *Eur. J. Org. Chem.*, 1998, 1743–1757.
93 K. A. Nielsen, J. O. Jeppesen, N. Thorup and J. Becher, *Org. Lett.*, 2002, **4**, 1327–1330.
94 K. A. Nielsen, J. O. Jeppesen, E. Levillain, N. Thorup and J. Becher, *Org. Lett.*, 2002, **4**, 4189–4192.
95 S. Bähring, K. R. Larsen, M. Supur, K. A. Nielsen, T. Poulsen, K. Ohkubo, C. W. Marlatt, E. Miyazaki, K. Takimiya, A. H. Flood, S. Fukuzumi and J. O. Jeppesen, *Chem. Commun*., 2017, **53**, 9898–9901.
96 H. Amouri, C. Desmarets and J. Moussa, *Chem. Rev*., 2012, **112**, 2015–2041.
97 B. Therrien, in Chemistry of Nanocontainers, Vol. 319 (Eds.: M. Albrecht and E. Hahn), Springer Berlin Heidelberg, 2012, pp. 35–55.
98 T. K. Ronson, S. Zarra, S. P. Black and J. R. Nitschke, *Chem. Commun*., 2013, **49**, 2476–2490.
99 R. Custelcean, *Chem. Soc. Rev*., 2014, **43**, 1813–1824.
100 M. Han, D. M. Engelhard and G. H. Clever, *Chem. Soc. Rev*., 2014, **43**, 1848–1860.
101 M. Fujita, J. Yazaki and K. Ogura, *J. Am. Chem. Soc.*, 1990, **112**, 5645–5647.
102 P. J. Stang and D. H. Cao, *J. Am. Chem. Soc*., 1994, **116**, 4981–4982.
103 M. Ferrer, A. Pedrosa, L. Rodríguez, O. Rossell and M. Vilaseca, *Inorg. Chem*., 2010, **49**, 9438–9449.
104 B. Lippert and P. J. Sanz Miguel, *Chem. Soc. Rev*., 2011, **40**, 4475–4487.
105 S. Goeb, S. Bivaud, P. I. Dron, J.-Y. Balandier, M. Chas and M. Sallé, *Chem. Commun*., 2012, **48**, 3106–3108.
106 J.-Y. Balandier, M. Chas, S. Goeb, P. I. Dron, D. Rondeau, A. Belyasmine, N. Gallego and M. Sallé, *New J. Chem*., 2011, **35**, 165–168.
107 S. Bivaud, J. Y. Balandier, M. Chas, M. Allain, S. Goeb and M. Sallé, *J. Am. Chem. Soc*., 2012, **134**, 11968–11970.
108 S. Bivaud, S. Goeb, J. Y. Balandier, M. Chas, M. Allain and M. Sallé, *Eur. J. Inorg. Chem*., 2014, 2440–2448.

109 S. Goeb, S. Bivaud, V. Croué, V. Vajpayee, M. Allain and M. Sallé, *Materials* 2014, **7**, 611–622.
110 V. Vajpayee, S. Bivaud, S. Goeb, V. Croué, M. Allain, B. V. Popp, A. Garci, B. Therrien and M. Sallé, *Organometallics* 2014, **3**3, 1651–1658.
111 A. J. Moore and M. R. Bryce, *J. Chem. Soc. Perkin Trans.1* 1991, 157–168.
112 M. R. Bryce, A. J. Moore, M. Hasan, G. J. Ashwell,A. T. Fraser, W. Clegg, M. B. Hursthouse and A. I. Karaulov, *Angew. Chem., Int. Ed.*, 1990, **29**, 1450–1452.
113 Y. Yamashita, Y. Kobayashi and T. Miyashi, *Angew. Chem., Int. Ed.*, 1989, **28**, 1052–1053.
114 S. Bivaud, S. Goeb, V. Croué, P. I. Dron, M. Allain and M. Sallé, *J. Am. Chem. Soc.*, 2013, **135**, 10018–10021.
115 V. Croué, S. Goeb, G. Szalóki, M. Allain and M. Sallé, *Angew. Chem., Int. Ed.*, 2016, **55**, 1746–1750.
116 S. Bivaud, S. Goeb, V. Croué, M. Allain, F. Pop and M. Sallé, *Beilstein J. Org. Chem*., 2015, **11**, 966–971.
117 G. Szalóki, V. Croué, M. Allain, S. Goeb and M. Sallé, *Chem. Commun.*, 2016, **52**, 10012–10015.
118 G. Szalóki, V. Croué, V. Carré, F. Aubriet, O. Aleveque, E. Levillain, M. Allain, J. Arago, E. Orti, S. Goeb and M. Sallé, *Angew. Chem., Int. Ed*., 2017, **56**, 16272–16276.
119 J. Su, S. Yuan, H.-Y., Wang, L. Huang, J.-Y. Ge, E. Joseph, J. Qin, T. Cagin, J.-L. Zuo and H.-C. Zhou, *Nat. Commun*., 2017, **8**, 2008.
120 T. C. Narayan, T. Miyakai, S. Seki and M. Dincă, *J. Am. Chem. Soc.*, 2012, **134**, 12932–12935.
121 S. S. Park, E. R. Hontz, L. Sun, C. H. Hendon, A. Walsh, T. van Voorhis and M. Dincă, *J. Am. Chem. Soc.*, 2015, **137**, 1774–1777.
122 S. S. Park, C. H. Hendon, A. J. Fielding, A. Walsh, M. O'Keeffe and M. Dincă, *J. Am. Chem. Soc.*, 2017, **139**, 3619–3622.
123 S. S. Park, A. J. Rieth, C. H. Hendon and M. Dincă, *J. Am. Chem. Soc.*, 2018, **140**, 2016–2019.
124 H.-Y. Wang, J.-Y. Ge, C. Hua, C.-Q. Jiao, Y. Wu, C. F. Leong, D. M. D'Alessandro, T. Liu and J.-L. Zuo, *Angew. Chem., Int. Ed*., 2017, **56**, 5465–5470.
125 H.-Y. Wang, L. Cui, J.-Z. Xie, C. F. Leong, D. M. D'Alessandro and J.-L. Zuo, *Coord. Chem. Rev*., 2017, **345**, 342–361 and the references therein.
126 B. Chen, Z.-P. Lv, C. F. Leong, Y. Zhao, D. M. D'Alessandro and J.-L. Zuo, *Cryst. Growth Des.*, 2015, **15**, 1861–1870.
127 H.-Y. Wang, Y. Wu, C. F. Leog, D. M. D'Alessandro and J.-L. Zuo, *Inorg. Chem*., 2015, **54**, 10766–10775.
128 M. Souto, A. Santiago-Portillo, M. Palomino, I. J. Vitórica-Yrezábal, B. J. C. Vieira, J. C. Waerenborgh, S. Valencia, S. Navalón, F. Rey, H. García and G. M. Espallargas, *Chem. Sci*., 2018, **9**, 2413–2418.
129 X. Feng, X. Ding and D. Jiang, *Chem. Soc. Rev.*, 2012, **41**, 6010–6022.
130 S.-Y. Ding and W. Wang, *Chem. Soc. Rev.*, 2013, **42**, 548–568.
131 S.-L. Cai, Y. -B. Zhang, A. B. Pun, B. He, J. Yang, F. M. Toma, I. D. Sharp, O. M. Yaghi, J. Fan, S. -R. Zheng, W.-G. Zhang and Y. Liu, *Chem. Sci.*, 2014, **5**, 4693–4700.
132 H. Ding, Y. Li, H. Hu, Y. Sun, J. Wang, C. Wang, C. Wang, G. Zhang, B. Wang, W. Xu and D. Zhang, *Chem. – Eur. J.*, 2014, **20**, 14614–14618.
133 S. Jin, T. Sakurai, T. Kowalczyk, S. Dalapati, F. Xu, H. Wei, X. Chen, J. Gao, S. Seki, S. Irle and D. Jiang, *Chem. – Eur. J.*, 2014, **20**, 14608–14613.
134 W.-l. Dong, L. Wang, H.-m. Ding, L. Zhao, D. Wang, C. Wang and L.-J. Wan, *Langmuir*, 2015, **31**, 11755–11759.
135 W.-L. Dong, S.-Y. Li, J.-Y. Yue, C. Wang, D. Wang and L.-J. Wan, *PCCP*, 2016, **18**, 17356–17359.
136 Z.-T. Li and J. Becher, *Chem. Commun.*, 1996, 639–640.
137 M. B. Nielsen, Z.-T. Li and J. Becher, *J. Mater. Chem*., 1997, 1175–1187.
138 D. Cao, M. Amelia, L. M. Klivansky, G. Koshkakaryan, S. I. Khan, M. Semeraro, S. Silvi, M. Venturi, A. Credi and Y. Liu, *J. Am. Chem. Soc*., 2010, **132**, 1110–1122.
139 M. Asakawa, P. R. Ashton, V. Balzani, A. Credi, C. Hamers, G. Mattersteig, M. Montalti, A. N. Shipway, N. Spencer, J. F. Stoddart, M. S. Tolley, M. Venturi, A. J. P. White and D. J. Williams, *Angew. Chem., Int. Ed*., 1998, **37**, 333–337.
140 C. P. Collier, G. Mattersteig, E. W. Wong, Y. Luo, K. Beverly, J. Sampaio, F. M. Raymo, J. F. Stoddart and J. R. Heath, *Science,* 2000, **289**, 1172–1175.
141 K. E. Griffiths and J. F. Stoddart, *Pure Appl. Chem.*, 2008, **80**, 485–506.
142 J. M. Spruell, A. Coskun, D. C. Friedman, R. S. Forgan, A. A. Sarjeant, A. Trabolsi, A. C. Fahrenbach, G. Barin, W. F. Paxton, S. K. Dey, M. A. Olson, D. Benítez, E. Tkatchouk, M. T. Colvin, R. Carmielli, S. T. Caldwell, G. M. Rosair, S. G. Hewage, F. Duclairoir, J. L. Seymour, A. M. Z. Slawin, W. A. Goddard III, M. R. Wasielewski, G. Cooke and J. F. Stoddart, *Nat. Chem.*, 2010, **2**, 870–879.
143 A. Coskun, J. M. Spruell, G. Barin, A. C. Fahrenbach, R. S. Forgan, M. T. Colvin, R. Carmieli, D. Benítez, E. Tkatchouk, D. C. Friedman, A. A. Sarjeant, M. R. Wasielewski, W. A. Goddard III and J. F. Stoddart, *J. Am. Chem. Soc*., 2011, **133**, 4538–4547.
144 G. Koshkakaryan, K. Parimal, J. He, X. Zhang, Z. Abliz, A. H. Flood and Y. Liu, *Chem. – Eur*. J., 2008, **14**, 10211–10218.
145 M. Frasconi, T. Kikuchi, D. Cao, Y. Wu, W.-G., Liu, S. M. Dyar, G. Barin, A. A. Sarjeant, C. L. Stern, R. Carmieli, C. Wang, M. R. Wasielewski, W. A. Goddard III and J. F. Stoddart, *J. Am. Chem. Soc.*, 2014, **136**, 11011–11026.
146 C. Cheng, P. R. McGonigal, J. F. Stoddart and R. D. Astumian, *ACS Nano*, 2015, **9**, 8672–8688 and the references therein.
147 G. Yu, B. C. Yung, Z. Zhou, Z. Mao and X. Chen, *ACS Nano*, 2018, **12**, 7–12 and the references therein.
148 R. J. Brea, L. Castedo, J. R. Granja, M. A. Herranz, L. Sánchez, N. Martín, W. Seitz and D. M. Guldi, *Proc. Natl. Acad. Sci., U. S. A.,* 2007, **104**, 5291–5294.
149 M. Schnippering, A. Zahn, S.-X. Liu, C. Leumann, S. Decurtins and D. J. Fermín, *Chem. Commun*., 2009, 5552–5554.
150 C. Colomban, C. Fuertes-Espinosa, S. Goeb, M. Sallé, M. Costas, L. Blancafort and X. Ribas, *Chem. – Eur. J.*, 2018, **24**, 4371–4381.
151 A. López-Andarias, J. López-Andarias, C. Atienza, F. J. Chichón, J. L. Carrascosa and N. Martín, *Chem. – Eur. J.,* 2018, **24**, 7755–7760.
152 J. Rebek, Jr. *Acc. Chem. Res.*, 1990, **23**, 399–404.

Author information

Biographies

Atanu Jana received his Ph.D. in Supramolecular Chemistry from IIT Kanpur, India, in 2010 under Professor Parimal K. Bharadwaj. Then he did a postdoc with Professor Jonathan L. Sessler at Yonsei University (Seoul). After that he moved to NIMS, Japan, and worked with Dr. Jonathan P. Hill and Professor Katsuhiko Ariga before joining Professor Michael D. Ward's Group at University of Sheffield, UK, as a Marie Curie International Incoming Research Fellow. He is now working with Professor Sessler in Shanghai University. His research interests focus on macrocyclic materials constructed using TTF-calixpyrrole, exTTF-porphyrin and TTF-porphyrin synthons, and studies of their applications.

Jonathan L. Sessler received a B.Sc. degree in Chemistry in 1977 from the University of California, Berkeley. He obtained his Ph.D. from Stanford University in 1982. After postdoctoral stays in Strasbourg and Kyoto, he accepted a position as an Assistant Professor of Chemistry at the University of Texas at Austin, where he is currently the Doherty-Welch Chair. He was also a WCU Professor at Yonsei University and recently accepted a summer research professorship and laboratory directorate at Shanghai University. Professor Sessler is currently working on Supramolecular Chemistry, Drug Discovery, Soft Materials, and Expanded Porphyrin Chemistry. Homepage: http://sessler.cm.utexas.edu/Sessler_Group_Website/Home.html

Masatoshi Ishida received his Ph.D. degree from Kyushu University in 2010 under the supervision of Professor Yoshinori Naruta. After working as a research fellow at the Institute for Materials Chemistry and Engineering (IMCE), Kyushu University, he worked with Professors Jonathan L. Sessler and Dongho Kim as a WCU postdoctoral research fellow at Yonsei University, Korea. He is currently an Assistant Professor in the Department of Chemistry and Biochemistry and Center for Molecular Systems (CMS), Kyushu University, Japan. His current research interests are focused on the synthetic and redox chemistry of novel π-conjugated porphyrinoids.

The Odense team consists of **Steffen Bähring** (right) and **Jan O Jeppesen** (left).

Steffen Bähring received his Ph.D. in Supramolecular Chemistry from the University of Southern Denmark in 2013 under the guidance of Professors Kent A. Nielsen and Jan O. Jeppesen. During this time, he visited the Sessler lab (2011–2012). After his Ph.D., he worked at the Danish Technological Institute. Dr. Bähring was awarded a Danish Independent Postdoctoral Scholarship (2016–2018) to work on tetrathiafulvalene-based organic photovoltaics with Professors Jeppesen, Sessler and Guldi. In 2018, he became an Assistant Professor at the University of Southern Denmark.

Jan O. Jeppesen received his Ph.D. from the University of Southern Denmark in 2001 with Professor Jan Becher as his supervisor and Professor J. Fraser Stoddart from the University of California, Los Angeles as his co-supervisor. He is the recipient of the Ellen and Niels Bjerrum Chemistry Award (2014), Torkil Holm prize (2010),

Villum Kann Rasmussens award (2009), the Aksel Tovborg Jensens award (2009) and the Hede Nielsens prize (2003). He is currently Vice-Chairman of The Danish Council for Independent Research, Technology, and Production Sciences (FTP). Since 2008, he has been a Full Professor at the University of Southern Denmark. Homepage: http://www.jojgroup.sdu.dk

The Angers team consists of **David Canevet** (left), **Sébastien Goeb** (right) and **Marc Sallé** (middle).

David Canevet obtained his Ph.D. in 2010 under Professor Marc Sallé. After postdoctoral work with Professor Nazario Martin, he was appointed as Assistant Professor in the MOLTECH-Anjou laboratory (2011). His research interests involve π-functional foldamers and organogels.

Sébastien Goeb obtained his Ph.D. in 2006 under the supervision of Professors Raymond Ziessel and Antoinette De Nicola. After postdoctoral work with Professor Felix Castellano at Bowling Green State University, he became Chargé de Recherche CNRS in the MOLTECH-Anjou Laboratory (2008). His research interests concern supramolecular discrete architectures constructed through coordination driven self-assembly.

Marc Sallé received his Ph.D. from the University of Angers in 1991 under Professor Alain Gorgues. After a postdoctoral stay with Professor Martin R. Bryce at the University of Durham, he became an Assistant Professor at the University of Angers, and was promoted to a Professor in 1998. He was awarded the Dina Surdin prize and is a junior member of the Institut Universitaire de France and a Distinguished Senior member of the Société Chimique de France. He directs the MOLTECH-Anjou Laboratory. His research focuses on the Supramolecular Chemistry of electro(photo)-active molecular systems. Homepage: http://moltech-anjou.univ-angers.fr

TOC Graphic

Functionalised tetrathiafulvalene- (TTF-) macrocycles: Recent trends in applied supramolecular chemistry

Atanu Jana,[a] Steffen Bähring,[b] Masatoshi Ishida,[c] Sébastien Goeb,[d] David Canevet,[d] Marc Sallé,*[d] Jan O. Jeppesen*[b] and Jonathan L. Sessler*[ae]

[a]*Institute for Supramolecular Chemistry and Catalysis, Shanghai University, Shanghai, 200444, China.*
[b]*Department of Physics, Chemistry and Pharmacy, University of Southern Denmark, Campusvej 55, 5230, Odense M, Denmark. E-mail: joj@sdu.dk Telephone: +45-65502587.*
[c]*Department of Chemistry and Biochemistry, Graduate School of Engineering and Center for Molecular Systems, Kyushu University, Fukuoka 819-0395, Japan*
[d]*Université d'Angers, CNRS UMR 6200, Laboratoire MOLTECH-Anjou, 2 bd Lavoisier, 49045 Angers Cedex, France. E-mail : marc.salle@univ-angers.fr Telephone: +33-241735439.*
[e]*Department of Chemistry, University of Texas at Austin, Austin, Texas 78712-1224, USA. E-mail: sessler@cm.utexas.edu Telephone: +1-512-471-5009.*